North Atlantic atmospheric rivers in the ERA-Interim dataset: Detection, climatology and link to Swiss floods

Master's Thesis

Faculty of Science
University of Bern

presented by

Valérie Fazan

2014

Supervisor:

Prof. Dr. Olivia Romppainen-Martius
Institute of Geography of the University of Bern and Oeschger Centre for Climate Change Research, University of Bern

Advisor:

Paul Froidevaux
Institute of Geography of the University of Bern and Oeschger Centre for Climate Change Research, University of Bern

Abstract

Atmospheric rivers (ARs) are narrow corridors of high moisture fluxes extending from the tropics towards the mid-latitudes and can contribute to heavy precipitation and flood events in various regions. While North Pacific ARs have been the focus of many previous studies, North Atlantic ARs have remained poorly studied. Because of their influence on extreme events, it is of high interest to have a better understanding about the seasonality of ARs and their effects over land, especially in mountainous regions such as Switzerland, where orographic precipitation can occur. The present master's thesis aims at filling part of the gap in knowledge about North Atlantic ARs, as well as their impact in Europe. An algorithm detecting ARs in the ERA-Interim dataset between 1979 and 2011 was developed. It consists of four detection schemes which detect ARs according to various criteria (total precipitable water, wind speed, integrated water vapor and area). The algorithm also detects structures having shorter length than ARs ($< 2000\,\mathrm{km}$), which nevertheless bring significant amounts of moisture towards the land. We named these structures high integrated vapor transport areas (HIAs). Using the algorithm output, the seasonal climatological frequency of ARs/HIAs was computed for the period 1979-2011, with special focus given to the North Atlantic and European regions. While different seasonalities were observed depending on the detection schemes, the AR/HIA climatology showed a strong resemblance to the storm track climatology over the North Atlantic, as well as a seasonal shift in the AR/HIA frequency maxima. Based on the AR/HIA climatology, the seasonal and regional influence of ARs/HIAs on flood events in Switzerland was investigated. We found that both the topography and the direction of the flow influence the occurrence of floods in Switzerland when AR/HIA conditions are observed over the country. Two regions are particularly sensitive to ARs/HIAs: the Jura (NW Switzerland) in winter and spring and Ticino (S Switzerland) in fall and summer. Finally, the relation between ARs/HIAs and extratropical cyclones was investigated for the winter 1989-1990, by analyzing how the ARs/HIAs were associated with fronts and with warm conveyor belts (WCBs). A strong relation was found between ARs, extratropical cyclones and their related WCBs over the western North Atlantic. However, in the eastern North Atlantic two thirds of the ARs seemed to become decoupled from the WCBs, suggesting that while ARs and WCBs evolve together and are closely related, they are distinct features that should be distinguished from one another. In addition, some ARs were observed to be associated with multiple cyclones, which could be of high importance for the persistence of the ARs and for the transport of considerable amounts of moisture towards Europe.

Acknowledgments

First of all, I would like to thank my supervisor Olivia Romppainen-Martius for her time and support throughout this year and for giving me the opportunity to discover a fascinating topic. A big thank you also goes to my advisor Paul Froidevaux for all the time he devoted to answering my questions and for all the suggestions he gave regarding my work. Thank you also to Sebastian Schemm from the ETH Zurich for providing data, giving interesting propositions and answering all my interrogations and to Hanin Binder and Heini Wernli from the ETH Zurich for providing interesting data.

Special thanks also goes to Jonathan Bussard for his general support, corrections and comments, as well as to Laurence Fazan, Sagen Gearhart and Matthias Röthlisberger for taking the time to read and comment my thesis. Thank you also to Matthieu Reussner for his computer assistance throughout the years, to Donatus Berger who was always there to turn on my computer when needed, to the IT staff for their technical support and to all my colleagues who helped in a way or another for the achievement of this work. Finally, I would like to thank my family and extended family for their support in my academic and non academic life.

Contents

List of Figures

List of Tables

Chapter 1

Introduction

1.1 Motivation

Atmospheric moisture transport is an important component of the Earth's water cycle and energy budget. A large amount of moisture is found where temperatures are high at low latitudes, because of the increase of the saturated vapor pressure of the air with temperature (Godard and Tabeaud, 2009). Moisture is then transported from tropical regions towards higher latitudes, where water precipitates over the land and ocean. However, this transport is not homogeneous in space and time (Fig. 1.1). It has been shown that at any given time, more than 90% of the total poleward atmospheric moisture transport at mid-latitudes is concentrated in four or five narrow regions that represent less than 10% of the circumference of the Earth at those latitudes (Zhu and Newell, 1998). These features are known as atmospheric rivers (ARs). Their name refers to their filament-like structure and to the high water vapor transport occurring within them, which has similar magnitude as the water transport of big terrestrial rivers such as the Amazon (Stohl et al., 2008).

By transporting large amounts of moisture from tropical regions to the extratropics, ARs evidently have effects in the mid-latitudes when they make landfall. A first effect is their significant contribution to the water resource in coastal regions. On the U.S. West Coast for example, ARs produce 25-50% of the annual precipitation (Ralph and Dettinger, 2012). A second effect is their contribution to heavy precipitation and to floods, especially in regions with coastal mountains, where the moist air coming from the ocean is forced to rise over the relief, producing orographic precipitation (e.g. Ralph et al., 2006; Lavers et al., 2011; Neiman et al., 2011; Lavers et al., 2012; Ralph and Dettinger, 2012; Lavers and Villarini, 2013). In

addition, the effects of ARs are not only felt on the western coast of the continents but also further east. In Europe, for example, ARs can affect regions as far as Germany and Poland (Lavers and Villarini, 2013).

Therefore, because of their contribution to the occurrence of heavy precipitation and flood events in many regions, it is crucial to have a better understanding about the seasonality of ARs and their effects over land. This is of particular interest in mountainous regions such as Switzerland, where the mountain chains (Jura, Alps) play an important role on the lifting of air masses and the triggering of orographic precipitation (e.g. Massacand et al., 1998).

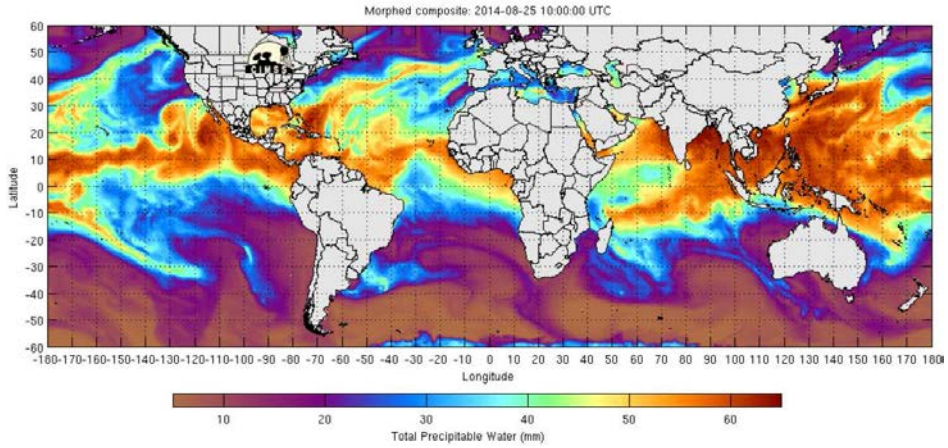

Figure 1.1: *Total precipitable water [mm] derived from the SSMI/SSMIS/TMI satellite passive microwave radiometers for 25 August 2014 10 UTC. AR structures are visible extending from the tropics towards the mid-latitudes, for example in the eastern North Pacific Ocean or in the North Atlantic Ocean. Taken from the Cooperative Institute for Meterological Satellite Studies, Tropical Cyclones Group (2014).*

1.2 State of research

An AR can be defined as a narrow corridor of air in which intense moisture transport takes place (Lavers and Villarini, 2013). While the transport of moisture in a narrow band within the low-level jet region of extratropical cyclones has been known for over forty years (e.g. Browning and Pardoe, 1973), it is only in the 90s that Newell et al. (1992) named theses fluxes "tropospheric rivers", which later became known as "atmospheric rivers". A few years later, Zhu and Newell (1998) showed that at any given time, four to five ARs could be

observed over the globe, which contributed to more than 90% of the total poleward moisture flux from the tropics to the mid-latitudes. At first, research on ARs was carried out only in specific locations using observations from radiosoundings and radar data (e.g. Browning and Pardoe, 1973). However, the satellite era and the emergence of global reanalysis at the end of the 20^{th} century brought new analysis tools, enlarging considerably the temporal and spatial scales of possible research. Since then, an increasing number of studies have been conducted using these new data, as well as airborne and ground-based observations, to gain insight on AR structures, their evolution and their effects on coastal regions. While at first, most of the research focused on ARs forming in the Pacific Ocean and landfalling on the West Coast of the U.S. (e.g. Ralph et al., 2004, 2005; Bao et al., 2006; Neiman et al., 2008b), studies later extended to other regions of the globe such as the North Atlantic Ocean (Stohl et al., 2008; Knippertz and Wernli, 2010), Europe (e.g. Lavers et al., 2011), Africa (Fink and Knippertz, 2003; Knippertz and Martin, 2005) and South America (Viale and Nuñez, 2011).

Many studies explored AR structures and characteristics such as their size and moisture content (e.g. Ralph et al., 2004, 2005), their moisture sources (e.g. Bao et al., 2006; Stohl et al., 2008; Knippertz and Wernli, 2010; Sodemann and Stohl, 2013) and the influence of El Niño Southern Oscillation on moisture transport (e.g. Ralph et al., 2005; Bao et al., 2006). In addition, an inventory of all landfalling ARs on the west coast of North America was produced (Neiman et al., 2008b) and a method to quantify the amplitude of any AR event was developed (Neiman et al., 2008a). Finally, a climatology of cold-season ARs reaching the west coast of the U.S. was produced very recently (Rutz et al., 2014), adding to the comprehension of the phenomenon and to the effects of landfalling ARs.

All these studies led to a better understanding of AR structures and to the definition of typical AR characteristics, allowing the detection of such patterns in satellite and reanalysis data. They are the following (after Ralph et al., 2004; Neiman et al., 2008b; Lavers et al., 2011; Ralph and Dettinger, 2011):

- High values of integrated vapor transport (IVT),
- Integrated water vapor (IWV) values of more than 2 cm,
- Wind speed between 0 and 2 km altitude greater than $12.5\,\mathrm{m\,s^{-1}}$,
- Specific size that is more than 2000 km long and less than 1000 km wide.

It was also found that ARs are located in the lower troposphere and that in most cases they occur in the warm sector of extratropical cyclones, in the low-level jet region just ahead of the cold front (e.g. Ralph et al., 2004, 2005; Bao et al., 2006; Ralph and Dettinger, 2011) (Fig. 1.2). However, case studies have also shown that ARs can be formed by other

mechanisms, developing for example in the vicinity of tropical cyclones (Cordeira et al., 2013) or during the extratropical transition of tropical cyclones (Stohl et al., 2008).

Furthermore, it was shown that the moisture contained in ARs stems from two sources: (1) a direct poleward moisture transport from the tropics and (2) local moisture convergence within extratropical cyclones (Bao et al., 2006). While it was found that ARs often, but not always, originate in the tropics (e.g. Neiman et al., 2013), local moisture convergence and evaporation then become essential for the maintenance of the ARs, to compensate for the depletion of moisture due to precipitation along their paths (Cordeira et al., 2013).

The defining AR criteria presented above can easily be used in detection algorithms (e.g. Byna et al., 2011) and numerical models (e.g. Jankov et al., 2009; Leung and Qian, 2009) to track landfalling ARs and investigate their effects on coastal regions. Therefore, in recent years, research has not only focused on describing and understanding the AR phenomenon, but also aimed at determining the connection between ARs and heavy precipitation and flood events in coastal regions, as much in the eastern North Pacific as in the eastern North Atlantic. Findings have shown that in almost all cases, the largest fall and winter floods were related to landfalling ARs that caused an orographic enhancement of precipitation (e.g. Ralph et al., 2006; Lavers et al., 2011; Neiman et al., 2011; Lavers et al., 2012; Ralph and Dettinger, 2012; Lavers and Villarini, 2013). Furthermore, studies in the U.S. and in Europe have shown that ARs not only impact coastal regions, but that their effects can also extend further inland (e.g. Moore et al., 2012; Lavers and Villarini, 2013; Neiman et al., 2013). While research has mainly focused on the North Pacific and North Atlantic Oceans, studies have also investigated the link between tropical moisture transport and heavy precipitation events in other regions of the world, for example in the Andes (Viale and Nuñez, 2011), in Morocco (Fink and Knippertz, 2003) or in tropical and subtropical West Africa (Knippertz and Martin, 2005).

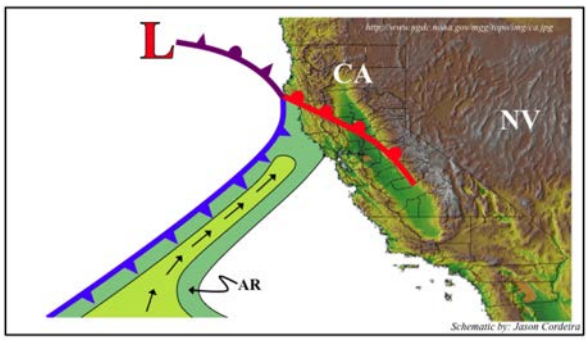

Figure 1.2: *Illustration of a landfalling AR (in green), located in the warm sector of an extratropical cyclone. The arrows indicate the direction of moisture transport. Taken from Cordeira (2014).*

Moreover, with increasing concern about the effects of climate change on the occurrence of extreme weather events, researchers have also started to model ARs and to investigate changes in AR frequency and intensity in the future in a changing climate. Lavers et al. (2013) showed that North Atlantic ARs were projected to increase in number and intensity, resulting in stronger rainfalls and bigger and more numerous flood events. In a study on Pacific ARs, Dettinger (2011) found that the season with the most ARs was projected to increase in length, resulting in a longer flood-prone period.

Finally, one should mention that the term "atmospheric river" has been criticized by some authors, because it suggests a two dimensional movement, whereas moisture transport within ARs should rather be seen as a three dimensional movement. These authors prefer the term "moisture conveyor belt" (e.g. Bao et al., 2006; Knippertz and Martin, 2007), which is more in accordance with the well-known conveyor belt model of extratropical cyclones and represents better the transport of moisture within ARs. Nevertheless, in this work we refer to these structures as ARs, since it is the term the most commonly used in the literature.

1.3 Research questions

Although research has widely studied AR structures and characteristics from a dynamical point of view, as well as the contribution of ARs to heavy precipitation and flood events in different regions of the world, focus has mainly been given to North Pacific ARs. In addition, studies of North Atlantic ARs have often focused on specific regions (e.g. the British Isles, Lavers et al., 2011, 2012) and on short time periods (e.g. Stohl et al., 2008; Sodemann and Stohl, 2013). Therefore, this master's thesis aims at filling part of the gap in knowledge about North Atlantic ARs, by providing a climatological study on a longer time period (1979-2011), as well as by investigating the effects of ARs over land in a mountainous region such as Switzerland. To do so, an algorithm consisting of different detection schemes has been developed in order to detect ARs in the ERA-Interim dataset (1979-2011). Using the algorithm output, our research then focuses on three main goals:

(1) The establishment of a climatology of North Atlantic ARs over a 32-year time period (1979-2011).

(2) The study of the seasonal and regional influence of ARs on flood events in Switzerland, given the susceptibility of the country to be affected by ARs, the mountain chains (Jura, Alps) playing an important role on the lifting of air masses and the triggering of orographic precipitation (e.g. Massacand et al., 1998).

(3) The study of the relation between ARs and extratropical cyclones, in particular how and to what extent they are related to fronts and to warm conveyor belts (WCBs), since ARs occur mostly within extratropical cyclones (Ralph et al., 2004, 2005; Bao et al., 2006; Ralph and Dettinger, 2011).

In the detail, we want to address the following questions:

- Does the algorithm detect AR structures well? What are its limitations and what detection schemes can be used for further studies?
- What is the seasonal climatological frequency of ARs over the North Atlantic Ocean and Europe for the period 1979-2011 as detected by the algorithm? During which season(s) are ARs most prevalent?
- To what extent do ARs influence flood events in Switzerland? Do we observe seasonal and/or regional disparities and how can they be explained?
- How are ARs associated with extratropical cyclones? Do ARs always occur simultaneously with fronts and WCBs or can they be linked to other processes?

The thesis is structured as follows: in Chapter 2, the different datasets used for the study are presented. In Chapter 3, the methods applied for the creation of the AR detection algorithm and for the different analyses are described. The results are presented in different sections in Chapter 4 and discussed following the same structure in Chapter 5. Finally, the main findings are summarized in Chapter 6 and ideas for further studies are presented in Chapter 7.

Chapter 2

Data

Four different datasets were used in this study and are briefly described in the following sections. They include the ERA-Interim reanalysis dataset from the European Center for Medium-Range Weather Forecasts (ECMWF), data on floods from the Federal Office for the Environment (FOEN), as well as front and warm conveyor belt data from the Institute for Atmospheric and Climate Science of the ETH Zurich.

2.1 ECMWF reanalysis data

The first dataset used is the ERA-Interim reanalysis dataset (Dee et al., 2011) from the European Center for Medium-Range Weather Forecasts (ECMWF). ERA-Interim is the latest reanalysis produced of ECMWF and contains improvements compared to previous products (e.g. ERA-40, Uppala et al., 2005). It covers the years 1979 up to present and has a spatial resolution of 0.75x0.75 latitude/longitude and is interpolated to a horizontal grid of 1° by 1°. The temporal resolution for atmospheric parameters is of 6 hours (Berrisford et al., 2009).

This dataset directly provides different atmospheric variables that are used for the AR detection algorithm such as the pressure or the zonal and meridional wind field. Other variables have to be calculated:

- The total precipitable water (TPW [$\mathrm{kg\,m^{-2}}$]) is calculated from 1000 to 0 hPa as in equation 2.1, where g is the acceleration due to gravity, q is the specific humidity, q_l and q_i are the cloud liquid and ice water contents and p is the pressure. This variable

was previously calculated by P. Froidevaux. One should note that the TPW is close to the integrated water vapor (IWV) since the integrated cloud water only represents a few percents of the TPW.

$$TPW = \frac{1}{g} \int_{1000}^{0\,hPa} (q + q_l + q_i)\, dp \tag{2.1}$$

- The integrated vapor transport (IVT [$\mathrm{kg\,m^{-1}\,s^{-1}}$]) is calculated between 1050 and 20 hPa as in equation 2.2, where g is the acceleration due to gravity, qu and qv are the zonal and meridional moisture fluxes and p is the pressure. The vertical integration of both moisture fluxes was previously calculated by P. Froidevaux.

$$IVT = \sqrt{(\frac{1}{g} \int_{1050}^{20\,hPa} qu\, dp)^2 \; + \; (\frac{1}{g} \int_{1050}^{20\,hPa} qv\, dp)^2} \tag{2.2}$$

- The absolute wind speed at a given pressure level ($\mathrm{m\,s^{-1}}$) is calculated as in equation 2.3, where u and v represent the zonal and meridional wind fields at a given pressure level.

$$speed = \sqrt{(u^2 + v^2)} \tag{2.3}$$

2.2 FOEN data

The second dataset was provided by the Federal Office for the Environment (FOEN). It consists of a list of dates with annual high water events and the corresponding discharge in $\mathrm{m^3\,s^{-1}}$ for more than 200 stations scattered over the Swiss territory for the period 1957-2012. The spatial distribution of the stations is represented in Fig. 3.1 (p. 15).

2.3 Front data

The third dataset is a front dataset, which was provided by the Institute for Atmospheric and Climate Science of the ETH Zurich. Frontal structures were detected in the ERA-Interim dataset by Schemm et al. (2014) according to a thermal method (for the complete description of the detection algorithm, see Schemm et al., 2014). This method identifies fronts by

calculating a parameter called the thermal frontal parameter (equation (1) in Schemm et al., 2014) using the equivalent potential temperature (θ_e) at 850 hPa as thermodynamic variable. A front is identified when the thermal frontal parameter is equal to zero. In addition, they exclude too weak thermal gradients by setting that the absolute gradient of θ_e must be greater than $4\,\mathrm{K}\,100\,\mathrm{km}^{-1}$. Finally, a length criterion is also applied. While the frontal patterns used for the analyses in this thesis are based on an earlier version of the algorithm, a new version was produced more recently using a different length criterion. The earlier version sets a minimum length of 10 grid points, while the later version sets a minimum length of 500 km, thus differences might be observed between the two versions.

2.4 Warm conveyor belt data

The last dataset, the warm conveyor belt (WCB) dataset, was also provided by the Institute for Atmospheric and Climate Science of the ETH Zurich. The original data is the WCB climatology of Madonna et al. (2014), who calculated trajectories with the ERA-Interim reanalysis data and identified WCBs as trajectories ascending by more than 600 hPa in 2 days in the vicinity of extratropical cyclones (for more information on this dataset and on WCBs, see Madonna et al., 2014). Using this data, H. Binder from the ETH Zurich identified preascending and ascending WCBs for the time period December 1989 - February 1990. For every time step, the horizontal position of the WCB trajectories in the ascending phase was noted. The ascending phase consisted of WCB trajectories ascending since 00, 06, 12, 18 and 24 hours. These horizontal positions were then projected onto a grid with a 1° by 1° horizontal resolution. The final product is a 6 hourly two-dimensional dataset containing ascending WCB density in units of number of WCBs/km^2. The same method was applied for WCB trajectories which were in the preascending phase. The preascending phase consisted of WCB trajectories that would ascend in the next 12, 24, 36, 48 and 60 hours following a given time step.

Chapter 3

Methods

In this chapter, the methods applied in this study are described. First, the AR detection algorithm and its different detection schemes are introduced (Section 3.1). Then, we explain how the seasonal climatological frequency of ARs was computed (3.2). Finally, we explain the steps followed to investigate the relation between ARs and flood events in Switzerland (3.3) and between ARs and extratropical cyclones (3.4).

3.1 Atmospheric river detection algorithm

As presented in Section 1.2, different studies resulted in the definition of typical AR characteristics, allowing an easy detection on weather maps or with satellite and reanalysis datasets. These criteria are the following (after Ralph et al., 2004; Neiman et al., 2008b; Lavers et al., 2011; Ralph and Dettinger, 2011):

- Integrated water vapor content (IWV) $\geq 20\,\mathrm{mm}$,
- Wind speed at low levels, i.e. between 0-2 km a.s.l., $\geq 12.5\,\mathrm{m\,s^{-1}}$,
- Integrated vapor transport (IVT) $\geq$ a given threshold,
- Long and narrow structure, i.e. length $\geq 2000\,\mathrm{km}$ and width $\leq 1000\,\mathrm{km}$.

For the IVT, no unique threshold exists, since values can vary considerably between study zones. Some analyses use fixed values (e.g. $250\,\mathrm{kg\,m^{-1}\,s^{-1}}$, Rutz et al., 2014), while others use statistical values (e.g. the 85^{th} percentile of IVT in a given latitude bin, Lavers et al., 2012).

Based on these definitions, five different AR detection schemes were created, in order to detect AR structures in the ERA-Interim dataset. The schemes are the following:

- TPW_{20}: detects structures with TPW $\geq 20\,\mathrm{mm}$ and wind speed at 750 hPa $\geq 12.5\,\mathrm{m\,s^{-1}}$,
- IVT_{350}: detects structures with IVT $\geq 350\,\mathrm{kg\,m^{-1}\,s^{-1}}$,
- IVT_{250}: detects structures with IVT $\geq 250\,\mathrm{kg\,m^{-1}\,s^{-1}}$,
- IVT_{p85}: detects structures with IVT $\geq 85^{th}$ percentile of IVT at a given grid point for a given month,
- IVT_{p95}: detects structures with IVT $\geq 95^{th}$ percentile of IVT at a given grid point for a given month.

For the first detection scheme, one should note that the TPW is close to the IWV which is usually used for AR detection, since the integrated cloud water only represents a few percents of the TPW. Thus differences should be small between this scheme and a similar scheme based on the IWV.

To obtain the percentiles of the IVT, the IVT values of all time steps for the period 1979-2011 at a given grid point were aggregated by month and the 85^{th} and 95^{th} percentiles were computed for each month. The illustration of the seasonal mean IVT values for the 85^{th} and 95^{th} percentiles are provided respectively in Fig. A.1 (Appendix) and in Fig. 4.2 (p. 22).

In addition, for all schemes, we decided to keep only patterns consisting of more than 30 grid cells to eliminate noise. This corresponds to roughly 263,000 $\mathrm{km^2}$ in the mid-latitudes. However, no other size or shape criteria were applied, in order to keep small structures which could bring considerable amounts of moisture towards the land, even though they are too small to be considered as ARs.

The algorithm was run for all days between 1979 and 2011 on a 6-hourly basis, i.e. for four time steps per day. For every grid point the criteria presented above were evaluated and results were written in a binary field. A "1" denoted the detection of AR characteristics, while a "0" indicated the absence of such a structure. This procedure was followed for all five detection schemes. The resulting data consisted of a file containing five variables (one for each detection scheme) and having a horizontal spatial resolution of 1° by 1° latitude/longitude.

3.2 Atmospheric river climatology

Using the algorithm output, the climatological frequency of ARs was computed for each season for the period 1979-2011. Since AR behavior should not change considerably within a season, differences being rather between the cold and the warm seasons (Gimeno et al., 2014), we decided to consider the seasonal time scale only. The seasons consisted of winter (DJF), spring (MAM), summer (JJA) and fall (SON). To obtain the seasonal frequencies, the AR data were summed up and averaged over all time steps, all days and all years within each season. Results had a spatial resolution of 1° by 1° latitude/longitude.

To compute the seasonal climatological frequency of ARs, two fixed-threshold-based detection schemes were used, TPW_{20} and IVT_{350}, because they were found to detect well AR structures over the North Atlantic Ocean (see Section 4.1). Since percentile-based schemes detect patterns occurring only a certain percentage of the time (for e.g. 15% for IVT_{p85}), there would have been no interest in computing frequencies using these schemes, since the resulting frequency values would not have shown any seasonality in AR activity. Finally, special attention was given to ARs occurring in the North Atlantic zone and over Europe, as it was the region of interest of this study.

3.3 Relation between atmospheric rivers and floods in Switzerland

To investigate the influence of ARs on floods in Switzerland, we first analyzed case studies of the fourteen largest flood events that occurred in the country between 1979 and 2011. Having found that ARs contribute in most cases to flooding, we then looked at smaller flood events, in order to determine the seasonal and regional influence of ARs on the occurrence of floods in Switzerland. The methods related to both analyses are explained in the following sections.

3.3.1 The fourteen largest flood events

Table 3.1 lists the dates of the fourteen largest flood events in Switzerland between 1979 and 2011. These dates were obtained from Froidevaux (2014), who took the dates of the large scale flood events identified by Schmocker-Fackel and Naef (2010) during that time

period (10 events) and added four other dates that were of particular interest (1991-12-22, 1999-05-22, 2000-08-06 and 2011-10-10) (Froidevaux, 2014). In total, fourteen cases were analyzed for the time period considered. For each event, plots of TPW, IVT, ARs (detected with schemes TPW_{20} and IVT_{350}), potential vorticity at different isentropic levels and daily precipitation were created for a period up to 10 days prior to the flood event. They were analyzed visually to determine if an AR was present near Switzerland on the day preceding or the day of the flood.

1987-07-19	1991-12-22	2000-08-06	2007-08-08
1987-08-25	1993-09-24	2000-10-16	2011-10-10
1987-09-27	1999-05-12	2002-08-12	
1990-02-15	1999-05-22	2005-08-22	

Table 3.1: *Dates representing the fourteen largest flood events in Switzerland between 1979 and 2011 that were used for this study.*

3.3.2 Smaller flood events

Next, we investigated the seasonal and regional influence of ARs on smaller flood events. Using the FOEN data (see Section 2.2), Froidevaux (2014) performed a block maxima method to obtain the dates with highest annual runoff at each measure station. In addition, the stations were classified into five regions according to their flood response to weather types (Froidevaux, 2014). The resulting regions are the Prealps, Eastern Switzerland, the Jura, Ticino and the Valais (Fig. 3.1). These regions have recently been updated and differences can be found compared to those presented in Froidevaux (2014). From this data, we chose to consider only dates with discharge having a return period larger than 5 years and occurring in three or more stations in a given region (thereafter referred to as flood days). This is motivated by the fact that some stations were classified in regions far from their geographical location. For e.g. the Aigle station, which is located in the Swiss Prealps, was classified in the Ticino region since floods in that station seem to be affected by the same weather types as Ticino stations. However, when high discharge events occurred upstream of this particular station in the Rhone valley, they were also measured in the Aigle station, thus contributing to a signal for Ticino, even in cases where little precipitation and low discharge were measured in that region, for e.g. in cases of NW flows. Hence, selecting events measured in more than three regions allows to counter this effect and to have a better regional representation of floods.

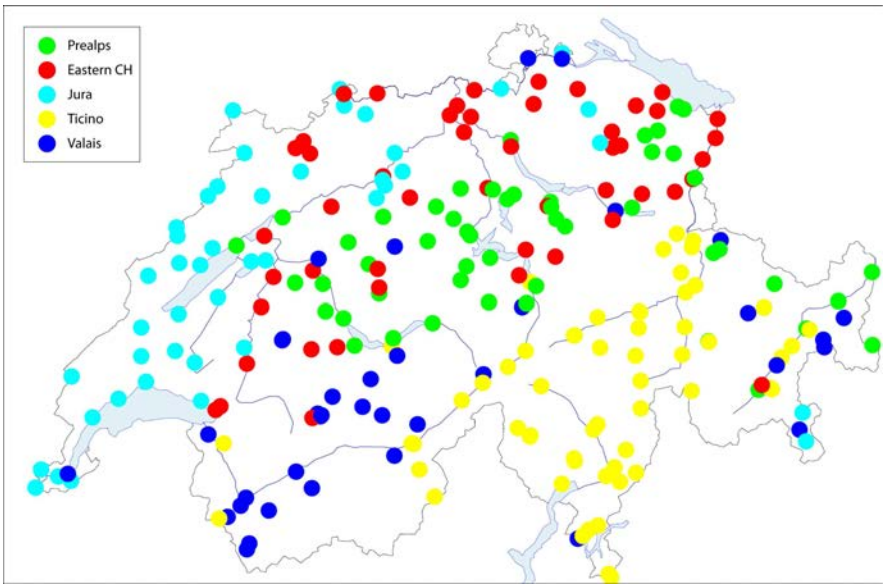

Figure 3.1: *Regional classification of the measure stations in Switzerland according to their flood response to weather types. Adapted from Froidevaux (2014).*

Table 3.2 presents the number of flood days and flood events per region and per season obtained with the date selection method. A distinction is made between flood days and flood events, since a given flood event can extend over several flood days. Floods separated by at least one day were considered as two separate events. The plots presented in Section 4.3.2 are based on individual flood days, while successive days were grouped into flood events to compute flood statistics (e.g. Tables 4.2 and 4.3 on pp. 28-29), in order to decrease the influence of long lasting events on the results. We decided to keep for further studies only seasons recording 8 or more floods events in a given region, as too few events lead to difficultly interpretable results. In addition, the Valais region was excluded, since it recorded too few flood events during every season.

The algorithm presented in Section 3.1 was then run again for the time period 1979-2011 with an additional criterion; instead of detecting the presence of an AR over a given grid point at a given time step, it searched this time for the presence of an AR at a given grid point over a 48 hour time period, i.e. on a given day and one day before. If AR characteristics were detected for at least one time step, a "1" was written in the data, while a "0" denoted the absence of such a structure. This additional criterion allowed us to account for the different response time of water basins to precipitation, which can vary according to the characteristics of the basins and is not always immediate. The algorithm was run only for percentile-based detection schemes IVT_{p85} and IVT_{p95}, because they were found to better detect moisture fluxes over land than fixed-threshold-based schemes (see Section 4.1).

	Winter		Spring		Summer		Fall		Total	
Prealps	0	0	2	2	**20**	**18**	3	3	25	23
Eastern CH	3	3	6	6	**17**	**15**	2	2	28	26
Jura	**12**	**8**	**8**	**8**	5	4	4	4	29	24
Ticino	0	0	1	1	**19**	**17**	**16**	**14**	36	32
Valais	0	0	1	1	3	2	4	4	8	7
Switzerland	**13**	**8**	18	12	61	50	29	25	121	95

Table 3.2: *Number of flood days (left) and flood events (right) per region and per season obtained with the date selection method for the period 1979-2011. Bold characters indicate flood days and flood events selected for further studies.*

In a next step, seasonal frequencies were computed using the new algorithm output for different time spans: for all days between 1979 and 2011 (reference period) and for all flood days in Switzerland as well as in the selected regions (represented in bold characters in Table 3.2), following the method presented in Section 3.2. To have a better representation of the deviation of AR occurrence during flood events compared to climatological conditions, frequency anomalies for each season were also calculated by dividing the AR frequency of occurrence in a given region by the frequency of the reference period.

To evaluate the quality of our algorithm detection method, flood events were also analyzed visually in a subjective verification, to identify the presence over Switzerland of an AR on the day or the days before the event occurred in a given region. The ARs were counted and the seasonal AR frequency was obtained by dividing for each season the number of ARs by the total number of flood events which occurred at that season. This allowed the comparison of the given results with the frequencies obtained with the algorithm output.

Finally, to understand the synoptic situations responsible for AR activity above Switzerland prior to flood events, seasonal composite plots of sea level pressure, geopotential height at 500 hPa, equivalent potential temperature at 850 hPa and potential vorticity at different isentropic levels were created for all flood events showing AR characteristics over the country on the day preceding or the day of the flood event for the time step of 06 UTC. In cases where the events consisted of successive flood days, the date of the event was represented by the date of the first day experiencing flooding in any region of Switzerland.

3.4 Relation between atmospheric rivers and extratropical cyclones

Since the literature presented ARs as mostly occurring ahead of the cold front in the warm sector of extratropical cyclones (e.g. Ralph et al., 2004), we wanted to investigate how the North Atlantic ARs detected by the algorithm were connected to extratropical cyclones, by looking at the relation between ARs, fronts and WCBs. The analysis was conducted in the form of a case study of the winter season 1989-1990 and the methods related to both analyses are explained in the following sections.

3.4.1 Atmospheric rivers and fronts

To investigate the relation between ARs and fronts, an overlap of ARs and mobile fronts was performed using a script provided by Schemm et al. (2014). The script evaluated the overlap of AR structures and fronts for each time step within the study period (December 1989 to Febraury 1990). When there was overlap at one or more grid points, the whole AR structure was kept and written in a new data file, while non-overlapping patterns were removed. Detected ARs were based on the output of detection schemes TPW_{20} and IVT_{350}, while frontal structures were taken from the front dataset (see Section 2.3).

Then, the overlapping ARs and fronts were plotted, as well as non-overlapping fronts, in order to evaluate the overlap method and to investigate the relation between ARs and fronts for the given time period. Finally, the frequency of ARs overlapping with fronts was computed for the winter 1989-1990 following the same method as for the AR climatology (Section 3.2). In addition, the frequency difference was calculated by subtracting the frequency of ARs overlapping with fronts by the frequency of all ARs for the same time period, in order to compare both frequency values.

3.4.2 Atmospheric rivers and warm conveyor belts

To investigate the relation between ARs, preascending and ascending WCBs, plots of ARs, fronts and WCBs for the winter 1989-1990 were created. ARs were based on the output of detection scheme TPW_{20} and WCBs were taken from the WCB dataset (see Section 2.4).

Then, an overlap of ARs and preascending and ascending WCBs was conducted, following the method described above (Section 3.4.1). This allowed us to compute the frequency of ARs overlapping with preascending and ascending WCBs for the winter 1989-1990, as well as the difference compared to the frequency of all ARs for the same time period, in a similar way as explained above for fronts.

Chapter 4

Results

In this chapter, the results are presented in four parts. First, an example of the algorithm output for the different detection schemes is illustrated (Section 4.1). Then, the AR climatology is presented (4.2). Next, the relation between ARs and floods in Switzerland is investigated through the analysis of the fourteen largest flood events recorded in the country between 1979 and 2011, as well as through the analysis of smaller events (4.3). Finally, the relation between ARs and extratropical cyclones is investigated through the analysis of the relation between ARs, fronts and WCBs in a case study of the winter 1989-1990 (4.4).

4.1 Atmospheric river detection algorithm

The first goal of our work was to write an AR detection algorithm and to compare results obtained with the different detection schemes, in order to keep the ones that showed good detection (see Section 3.1 for the description of the algorithm). An example of the algorithm output for a given day is presented in Fig. 4.1. It shows particularly well that the moisture content criterion (TPW $\geq 20\,\mathrm{mm}$) is mostly met in the tropics, while the wind speed criterion (wind speed $\geq 12.5\,\mathrm{m\,s^{-1}}$) is rather met in the extratropics. When a plume of moisture extends from the tropics into the extratropical zone and crosses a zone with wind speed exceeding $12.5\,\mathrm{m\,s^{-1}}$, an AR is detected according to detection scheme TPW_{20} (Fig. 4.1a).

We observe that both IVT_{350} and IVT_{250} (Fig. 4.1b,c) detect similar structures as TPW_{20}, but also detect many patterns in the tropics. Furthermore, IVT_{250} detects larger structures

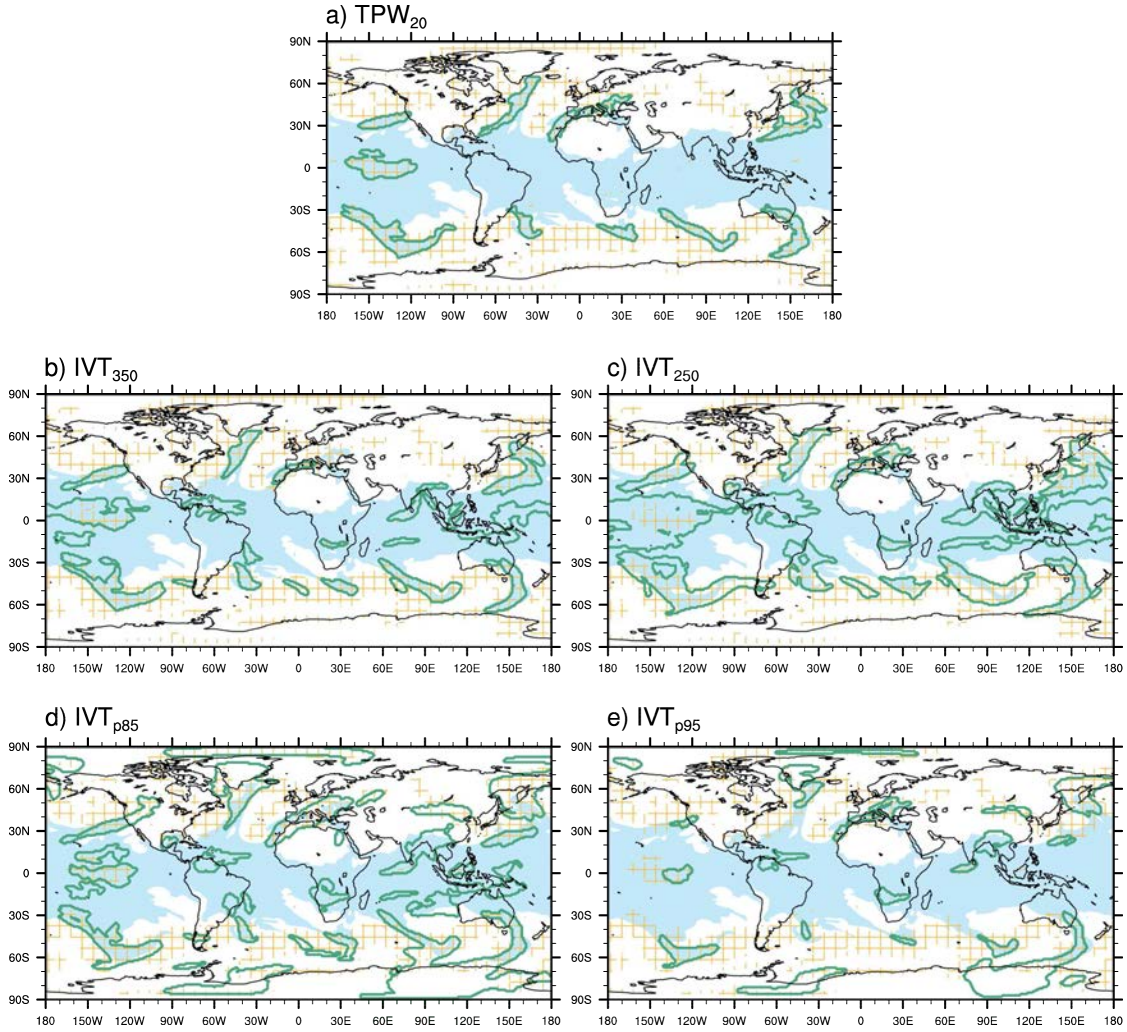

Figure 4.1: *ARs detected by the algorithm obtained with detection schemes (a) TPW_{20}, (b) IVT_{350}, (c) IVT_{250}, (d) IVT_{p85} and (e) IVT_{p95} for 09 December 2010 00 UTC, with $TPW \geq 20\,mm$ (blue shading), wind speed $\geq 12.5\,m\,s^{-1}$ (orange stipples) and detected ARs (green contour).*

than IVT_{350} and shows slight inland penetration. Schemes based on percentile thresholds IVT_{p85} and IVT_{p95} (Fig. 4.1d,e) also detect similar AR structures as the other schemes, as well as many patterns in the tropics. In addition, they detect patterns extending further inland than fixed-threshold-based schemes (e.g. over Antarctica, Greenland, the U.S. or Europe).

These observations allowed us to select four of the five detection schemes for further studies. Fixed-value-based schemes TPW_{20} and IVT_{350} were kept for the AR climatology (Section 4.2) and for the analysis of the relation between ARs and extratropical cyclones (Section 4.4), because they show good detection of ARs over the North Atlantic Ocean. Percentile-based schemes IVT_{p85} and IVT_{p95} were kept for the investigation of the influence

of ARs on floods in Switzerland (Section 4.3), because they detect AR patterns extending further over land than the other schemes. Finally, we decided not to keep IVT_{250} for further studies, since it detects similar patterns as the other schemes but shows smaller detection over land than percentile-based schemes, thus not providing any additional information.

Furthermore, we observed that the algorithm also detects structures over the North Atlantic Ocean and the Mediterranean Sea that do not meet all the defining AR characteristics presented in Section 1.2. Although these patterns have high TPW or IVT, they are too short ($< 2000\,\mathrm{km}$) to be considered as ARs. Therefore, they are thereafter referred to as "high IVT areas" (HIAs), to distinguish them from ARs as defined by the literature. They are especially observed in spring, summer and fall over the Mediterranean (see for Appendix Fig. A.4ab,f) and are better detected by schemes based on the IVT, which do not penalize for too low wind speeds. Although they have a shorter length than ARs, they can still bring considerable amounts of moisture towards the continent and are thus of interest when studying floods in different regions. Therefore, these patterns were not removed from the AR data.

When visually analyzing individual events, we also noted that over the Mediterranean Sea, the algorithm detects HIAs related to Vb situations (see Section 4.3.1). A Vb situation is characterized by the presence of a cyclone over the Golf of Genoa and moist air being advected in a cyclonic rotation from the Mediterranean towards eastern and central Europe. However, we noticed that not all of these structures are detected by the algorithm. Indeed, in many cases, the areas having TPW or IVT above the threshold fixed by the detection scheme are smaller than the 30 grid cells fixed by the size criterion and thus are not detected.

Fig. 4.2 and Fig. A.1 (Appendix) show the mean IVT values of the 95^{th} and 85^{th} percentiles of seasonal IVT used as thresholds by the percentile-based detection schemes. We observe seasonal and spatial variations over the North Atlantic and Europe. At all seasons, values are higher over the western North Atlantic and decrease eastwards. Over the North Atlantic (Figs. 4.2 and A.1 left), we observe a minimum of both percentiles in spring ($p_{85} < 400\,\mathrm{kg\,m^{-1}\,s^{-1}}$ and $p_{95} < 600\,\mathrm{kg\,m^{-1}\,s^{-1}}$), a maximum of p_{85} in summer (up to $615\,\mathrm{kg\,m^{-1}\,s^{-1}}$), and a maximum of p_{95} both in winter and in summer (up to $840\,\mathrm{kg\,m^{-1}\,s^{-1}}$). At a European scale (Figs. 4.2 and A.1 right), we also observe minimum IVT values in spring ($p_{85} < 250\,\mathrm{kg\,m^{-1}\,s^{-1}}$ and $p_{95} < 350\,\mathrm{kg\,m^{-1}\,s^{-1}}$) and maximum values over the continent in fall (p_{85} between 200-350 $\mathrm{kg\,m^{-1}\,s^{-1}}$ and p_{95} between 200-500 $\mathrm{kg\,m^{-1}\,s^{-1}}$), with even higher values over the British Isles.

We also notice that IVT values are lower over Switzerland and the Alps than in the neighboring countries. This could be either due to the moisture depletion of the air masses

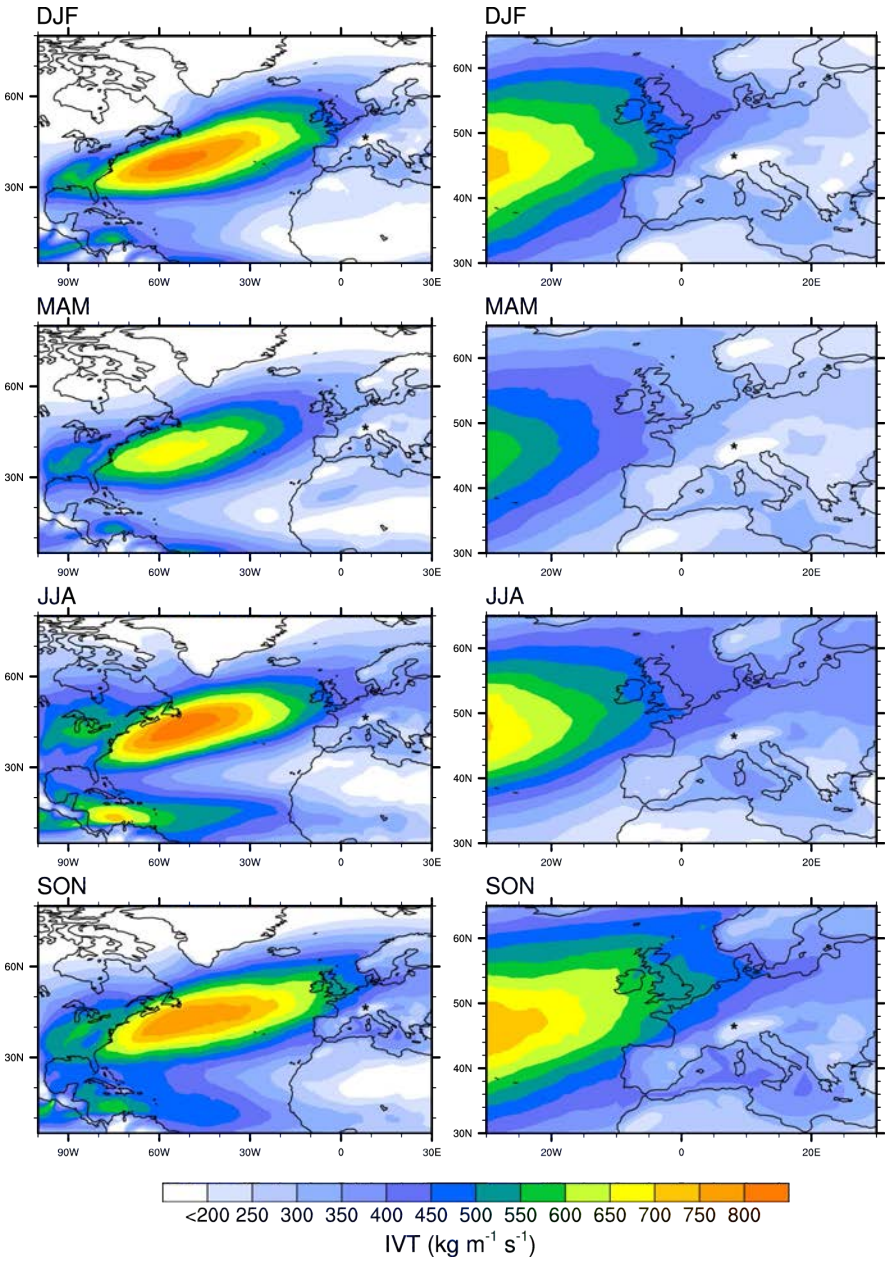

Figure 4.2: *95th percentile of seasonal IVT for (a) the North Atlantic and (b) Europe. The star indicates the location of Switzerland.*

as they rise over the Alps or due to the complex topography of Switzerland, which could be represented as a mountainous region by the reanalysis model. Since moisture in the atmosphere decreases with altitude, this could explain why IVT values are lower over the country. We observe $p_{85} < 250\,\mathrm{kg\,m^{-1}\,s^{-1}}$ in winter and spring and $< 300\,\mathrm{kg\,m^{-1}\,s^{-1}}$ in summer and fall, while p_{95} shows values $< 350\,\mathrm{kg\,m^{-1}\,s^{-1}}$ in winter and spring and $< 450\,\mathrm{kg\,m^{-1}\,s^{-1}}$ in summer and fall. If we compare these values with the threshold of the fixed-threshold-based detection scheme IVT_{350} (with a threshold at $350\,\mathrm{kg\,m^{-1}\,s^{-1}}$),

we notice that in summer and fall, the corresponding percentile value is between the 85^{th} and 95^{th} percentile, thus such a value is observed between 5 and 15% of the time over the country. In winter and spring, however, an IVT of $350\,\mathrm{kg\,m^{-1}\,s^{-1}}$ represents a percentile of 95 or higher, suggesting that such a value is observed less than 5% of the time. Therefore, depending on the season, the threshold fixed by the detection scheme represents different types of events. Over Switzerland, for example, it represents rare events in summer and fall, but only very rare events in winter and spring. Since the events detected by this scheme are more rare than those detected by the percentile-based schemes, the resulting AR patterns are also smaller, especially in winter and spring. IVT_{250}, which detects moisture fluxes occurring between 5 and 15% of the time in winter and spring and approximately 15% of the time in summer and fall, detects more common events, thus also bigger AR structures. Over the ocean, however, mean IVT values are higher and represent percentiles smaller than p_{85}, thus differences in detection between fixed-threshold-based schemes and percentile-based schemes are smaller.

4.2 Atmospheric river climatology

With the algorithm output, the seasonal climatological frequency of ARs/HIAs was computed for the time period 1979-2011 (see Section 3.2 for the method description and Section 4.1 for the definition of HIAs). Figs. 4.3 and 4.4 illustrate results obtained with detection scheme TPW_{20}, while figures for IVT_{350} can be found in the appendix (Figs. A.2 and A.3).

At a global level (Figs. 4.3 and A.2), both detection schemes show similar frequencies for the cold season at mid-latitudes, while IVT_{350} shows higher frequencies over the ocean in the warm season in both hemispheres. We also observe that in summer, both schemes detect monsoon patterns over India, as well as hurricane tracks in the Caribbean. Furthermore, the patterns detected by IVT_{350} in the tropics appear in the frequency plots, while TPW_{20} detects some patterns in winter in the tropical Pacific Ocean.

Focusing now on the North Atlantic Ocean (Figs. 4.4 and A.3 left), we observe that all seasons show a high frequency of ARs and HIAs over the western North Atlantic in the storm tracks (25 to 40%), with values decreasing when moving to the east. A minimum of AR and HIA activity is observed in spring ($< 30\%$), while maximal activity is found in winter and summer (up to 40%). Furthermore, the AR/HIA frequency maxima show seasonal variations, with a poleward shift in summer and an equatorward shift in winter, concomitant with the

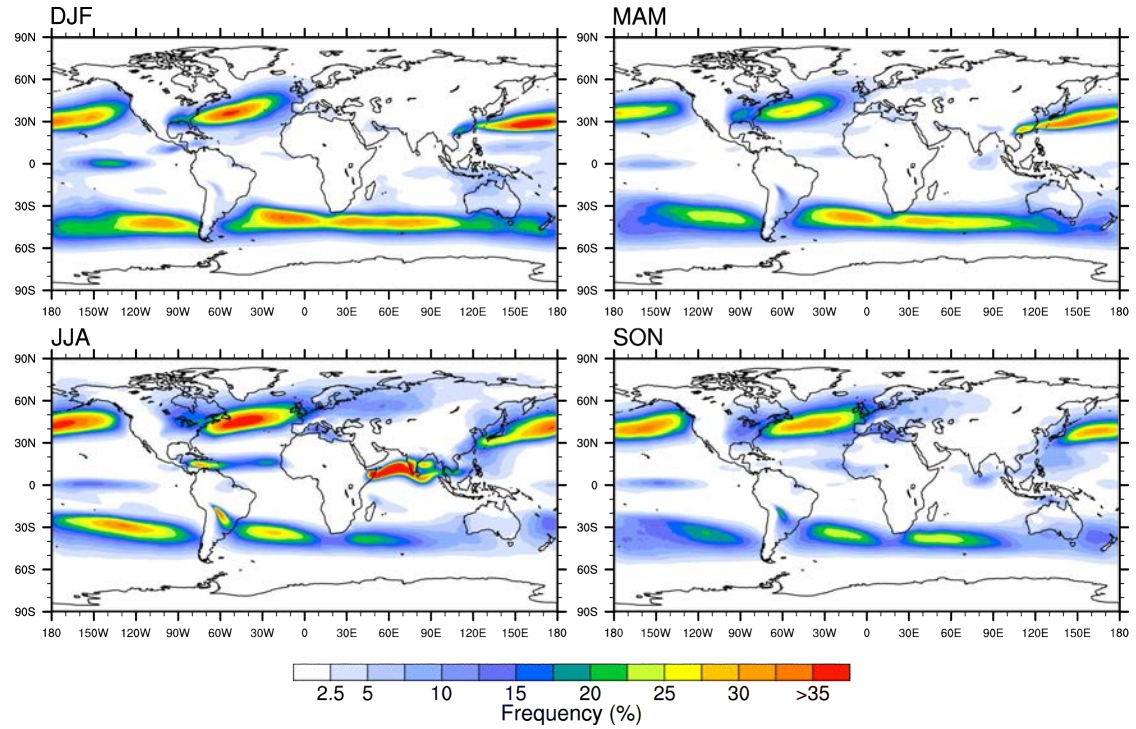

Figure 4.3: *Global seasonal frequency of ARs and HIAs for the period 1979-2011 obtained with detection scheme* TPW_{20}.

shift in storm tracks during these seasons. In addition, the orientation with which ARs approach the continent varies slightly with the season. These corridors of intense moisture transport appear to be more zonally oriented in summer and fall, approaching Europe in an almost westerly direction, while they have a SW-NE tilted orientation in winter and spring, reaching Europe in a southwesterly flow.

At a more regional scale (Figs. 4.4 and A.3 right), we observe that ARs and HIAs affect the European continent mostly in summer and in fall, with frequencies reaching 20%. Values are lower in winter and spring (up to 7.5%). The regions showing the highest frequency of occurrence of ARs and HIAs are the British Isles, northwestern France, Belgium, the Netherlands and the Mediterranean Sea. Over Switzerland, values are close to zero since the TPW and IVT over the country have low values (see Section 4.1). If we assume that moisture fluxes over Switzerland are similar to those over neighboring countries, we find that ARs and HIAs occur over Switzerland with a frequency of 5-7.5% in summer and fall and a frequency smaller than 2.5% in winter and spring. Hence, according to detection schemes TPW_{20} and IVT_{350}, these corridors of high moisture transport seem to rarely occur over this part of Europe, especially in winter and spring.

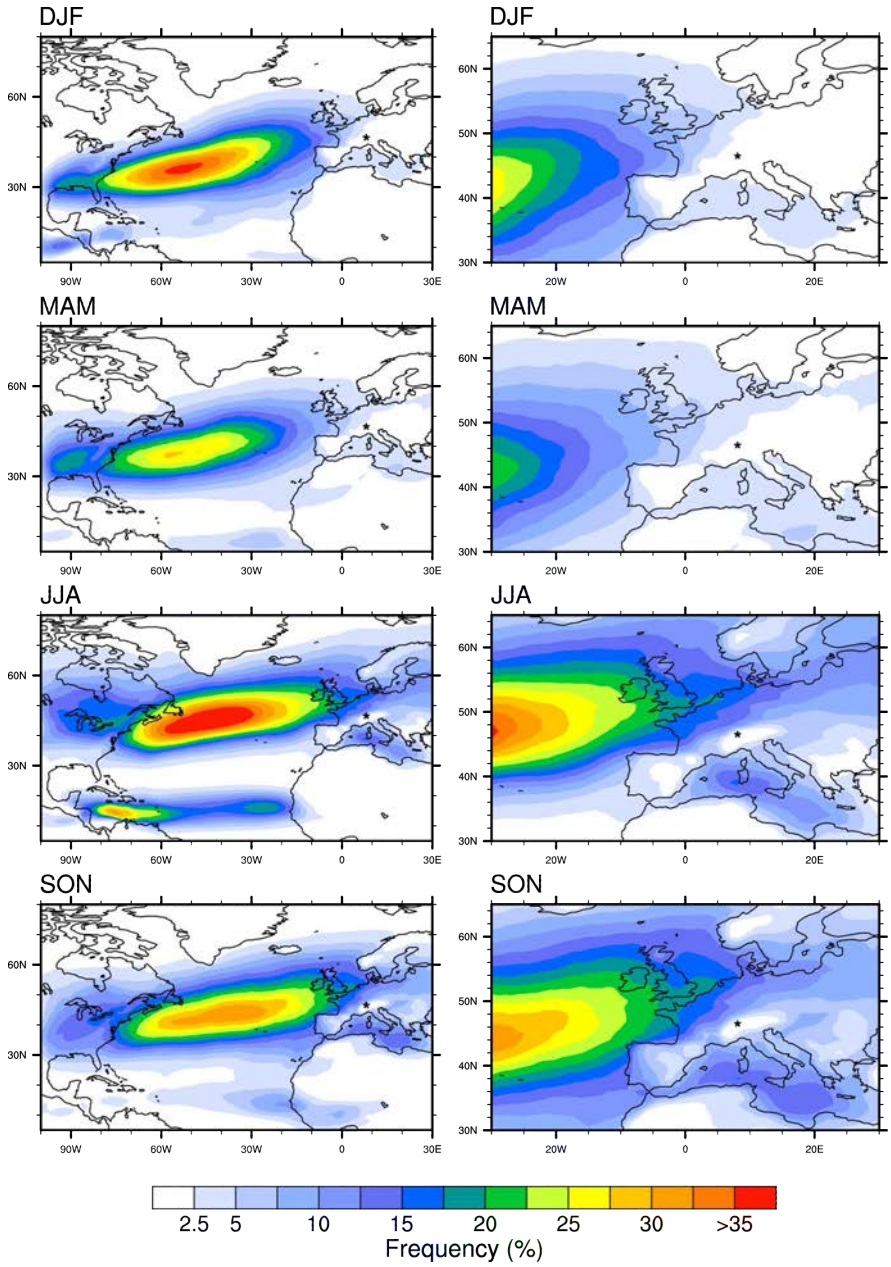

Figure 4.4: *Seasonal frequency of ARs and HIAs for the period 1979-2011 for the North Atlantic (left) and Europe (right) obtained with detection scheme* TPW_{20}*. The star indicates the location of Switzerland.*

4.3 Relation between atmospheric rivers and floods in Switzerland

The algorithm output also allowed us to investigate the influence of ARs/HIAs on flood events in Switzerland for the time period 1979-2011. This section describes first results concerning the fourteen largest flood events in Switzerland (Section 4.3.1), followed by smaller flood events (4.3.2). The definition of these events is presented in Section 3.3.

4.3.1 The fourteen largest flood events

For the fourteen largest flood events that occurred in Switzerland between 1979 and 2011 presented in Section 3.3.1, plots of TPW, IVT, ARs (detected with schemes TPW_{20} and IVT_{350}), potential vorticity at different isentropic levels and daily precipitation were created and analyzed. The analysis allowed the identification of the presence of ARs and HIAs over Switzerland prior to the occurrence of the events and the evaluation of the relevance of these corridors of high moisture transport to the triggering of floods. Results are summarized in Table 4.1 and plots of the fourteen cases can be found in the appendix (Figs. A.4a and A.4b). The analysis also showed that the algorithm is effective at detecting AR structures over the North Atlantic and Europe. We noticed that HIAs (the small advection patterns presented in Section 4.1) were detected over the Mediterranean Sea (Fig. A.4ab,f) and that some HIAs related to Vb situations are also detected (Fig. A.4bl) but not all of them (Figs. A.4ah and A.4bi). A Vb situation is characterized by the presence of a cyclone over the Golf of Genoa and moist air being advected in a cyclonic rotation from the Mediterranean towards eastern and central Europe, arriving in Switzerland in a NE flow. Even though HIAs related to Vb situations could follow similar processes as ARs but at a smaller scale, they are thereafter considered separately from ARs and other HIAs, since not all of these patterns are detected by the algorithm because of their small size, as explained in Section 4.1.

On a total of 14 events, 6 events occurred in summer (43%), followed by 4 events in fall (29%), 2 in winter (14%) and 2 in spring (14%). We noted that for 10 of these events, corridors of intense moisture transport over Switzerland could be observed the day or a few days prior to the flood event, either in ARs (8 events) or HIAs (2 events). The remaining events seemed be related to Vb situations (3 events) and to frontal activity (1 event). Hence, while all of the cold season floods show a relation with ARs or HIAs, only 50% of the warm season events can be related to such structures.

Datum	*Detected moisture fluxes near Switzerland*
1987-07-19	AR (SW flow)
1987-08-25	HIA (S flow)
1987-09-27	AR (SW-WSW flow)
1990-02-15	AR (W-WNW flow)
1991-12-22	AR (WNW-NW flow)
1993-09-24	HIA (S-SE flow)
1999-05-12	AR (W flow)
1999-05-22	Vb situation(N-NE flow)
2000-08-06	Vb situation (NE flow)
2000-10-16	AR first approaching the Mediterranean Sea in a westerly flow and then is fed by moisture coming from the south, shifting the AR into a southerly flow (WSW-SE flow)
2002-08-12	AR that passes over the Mediterranean and is then taken into a Vb situation (NW and NE flows)
2005-08-22	Vb situation, detected as a high IVT area (NE flow)
2007-08-08	Meeting of two air masses; the one advecting moist and warm air from the Mediterranean rises above the one advecting cold air from the north. Since the air masses flow in opposite directions, both flows cancel each other, resulting in low wind speeds visible on the plots.
2011-10-10	AR (NW flow)

Table 4.1: *Summary of the observed moisture fluxes near Switzerland and direction of advection on the day or the days prior to the fourteen largest flood events between 1979 and 2011.*

Since there seems to be a strong relation between ARs and flood events, especially during the cold season, we can now move to the analysis of smaller flood events, to analyze the influence of ARs/HIAs on these events.

4.3.2 Smaller flood events

The analysis of the influence of ARs/HIAs on smaller flood events was carried out following several steps. In a first step, (Section 4.3.2.1), the seasonal and regional distribution of smaller flood events in Switzerland was analyzed. These events, thereafter referred to as flood events, consist of all the events occurring between 1979 and 2011 with discharge having a return period larger than 5 years and being measured in three or more stations in a given region. In a second step (4.3.2.2), the seasonal influence of ARs and HIAs on floods in Switzerland and in the different regions was analyzed. In a third step (4.3.2.3), the frequencies obtained with the detection algorithm were compared with the frequencies obtained by visually counting the AR and HIA events, in order to verify the accuracy of the detection schemes. Finally in a last step (4.3.2.4), seasonal composite plots of flood-related ARs were produced, in order to gain insight on the synoptic situations responsible for AR occurrence over Switzerland on flood days.

4.3.2.1 Seasonal and regional distribution of flood events

The flood events selected for the analysis show different seasonal and regional distributions, presented in Tables 4.2 and 4.3. At a national scale, the seasonal distribution (Table 4.2) shows that most events occurred in summer (53%), followed by fall (26%), spring (13%) and winter (8%). At a regional scale, however, we notice different seasonal distributions. While the Jura seems to be more affected by floods in winter and spring (both 33%), Ticino shows a majority of events occurring in summer and fall (respectively 53% and 44%), the Valais a majority of events occurring in fall (57%) and the Prealps and Eastern Switzerland experienced most floods in summer (respectively 78% and 58%).

	Prealps	East CH	Jura	Ticino	Valais	**CH**
Winter	0%	12%	33%	0%	0%	**8**%
Spring	9%	23%	33%	3%	14%	**13**%
Summer	78%	58%	17%	53%	29%	**53**%
Fall	13%	8%	17%	44%	57%	**26**%
No. of events	23	26	24	32	7	**95**

Table 4.2: *Seasonal distribution of flood events for every region, based on the values found in Table 3.2 (p. 16).*

	Winter	Spring	Summer	Fall	**All seasons**
Prealps	0%	17%	36%	12%	**24%**
Eastern CH	38%	50%	30%	8%	**27%**
Jura	100%	67%	8%	16%	**25%**
Ticino	0%	8%	34%	56%	**34%**
Valais	0%	8%	4%	16%	**7%**
No. of events	8	12	50	25	**95**

Table 4.3: *Regional distribution of flood events for every season, based on the values found in Table 3.2 (p. 16).*

The regional distribution of flood events (Table 4.3) shows that at all seasons considered, most floods occurred in Ticino (34%), a similar amount in the Prealps, Eastern Switzerland and Jura regions (24-27%) and very few events in the Valais (7%). When looking at a seasonal scale, we notice regional differences. In winter, all floods occurring in Switzerland touched the Jura (100%), while Eastern Switzerland was less affected (38%) and all the other regions not affected (0%). In spring, the majority of the events touched the Jura (67%) and Eastern Switzerland (50%). In summer, floods equally affected the Prealps (36%), Ticino (34%) and to a smaller extent Eastern Switzerland (30%). Finally in fall, floods mostly occurred in the Ticino region (56%).

While the number of stations in each region can influence the number of flood events selected in the present study, the tables presented above give a first impression of the situation in Switzerland. Floods seem to have different seasonal and regional impacts; while the majority of the events occurred in summer (50 events) and in fall (25 events) and mostly affected Ticino, the Prealps and Eastern Switzerland, much fewer events occurred in spring (12 events) and in winter (8 events), which mostly affected the Jura and Eastern Switzerland. In the following section, we investigate whether these events could have been caused by the presence of ARs or HIAs over Switzerland on the day or the days prior to the events.

4.3.2.2 Seasonal and regional influence of atmospheric rivers on flood events in Switzerland

To analyze the seasonal and regional influence of ARs and HIAs on flood events in Switzerland, we first had to examine frequencies obtained with the algorithm output for the reference period, i.e. for all days between 1979 and 2011, since these values were used to compute

the anomalies of AR/HIA frequency on flood days compared to all days within the reference period. In Sections 4.1 and 4.2, the algorithm detected the presence of an AR/HIA over a given grid point at a given time step and percentile-based schemes detected IVT values occurring a certain percentage of the time (e.g. 15% for IVT_{p85}). There was no interest in computing frequencies of occurrence using these schemes, since the resulting frequencies would have been equal to the percentage represented by the percentile (e.g. 15%). In this section however, the algorithm searched for the presence of an AR/HIA at a given grid point over a 48 hour time period, i.e. on both the day preceding and the day of the flood event (see Section 3.4.2 for a complete description of the method). If at least one time step in the 48 hours showed AR/HIA characteristics at a given grid point, it was considered that an AR/HIA was present on the day of the flood at that grid point. Since eight time steps were considered, the algorithm detected higher frequencies as those presented in Section 4.2. Consequently, frequencies detected by percentile-based detection schemes were often higher than the percentage represented by the percentile (e.g. 15%). This allowed us to distinguish spatial and seasonal patterns in the frequency of ARs/HIAs over the North Atlantic and Europe for the reference period 1979-2011 (Appendix Fig. A.5). While the spatial patterns are similar to those presented in Section 4.1, seasonal patterns over the North Atlantic differ; we observe a higher frequency of ARs/HIAs in winter and fall and lower values in spring and summer. Over the European continent, however, seasonal differences are small. Near Switzerland, frequencies range between 10-20% (IVT_{p95}) and 30-40% (IVT_{p85}) at all seasons.

With these observations, we could then move to the seasonal analysis of the influence of ARs and HIAs on flood events in Switzerland and in the different regions. Fig. 4.5 shows the frequency of ARs/HIAs on both the day preceding and the day of a flood event was recorded in Switzerland obtained with detection scheme IVT_{p85}, as well as anomalies compared to the reference period. The corresponding plot for IVT_{p95} can be found in the appendix (Fig. A.6).

Winter events

On winter flood days, we observe clear AR/HIA signal over the North Atlantic and Europe. AR tracks seem to cross the ocean from SW to NE, bend southwards over southern Britain and cross western and central Europe in a NW-WNW flow (Fig. 4.5a). The anomaly plot (Fig. 4.5b) suggests a shift of AR tracks towards the south on flood days compared to climatological tracks, as well as increased AR/HIA activity over the continent. Over Switzerland, frequency values are high for both detection schemes, with 80-100% of the cases exhibiting ARs or HIAs on the day preceding or the day of the flood events. Anomalies range from 2.5 (IVT_{p85}) to >5 (IVT_{p95}), suggesting that on winter flood days ARs or HIAs were more than twice as frequent than for the reference period.

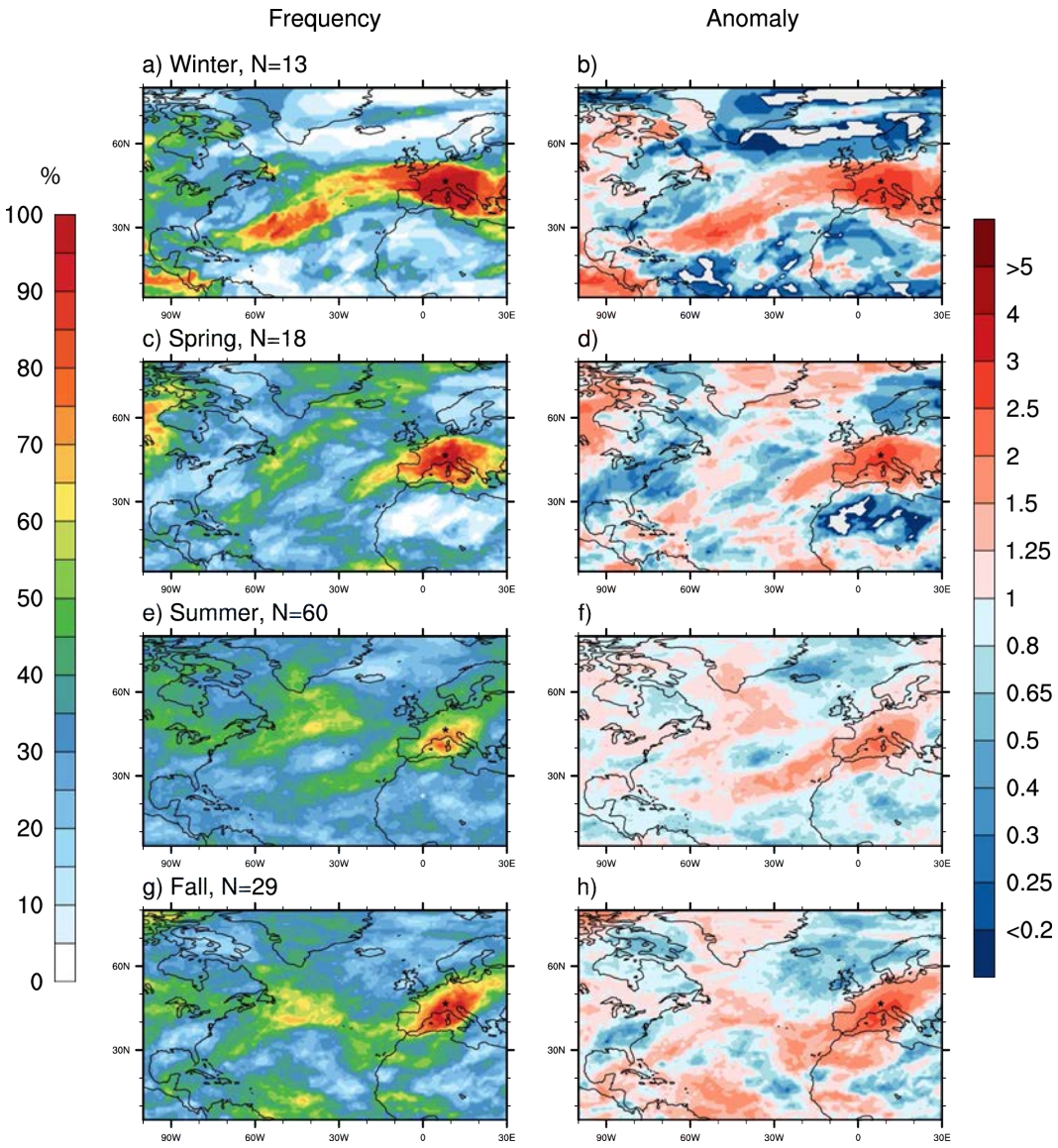

Figure 4.5: *Seasonal frequency of ARs and HIAs on the day preceding and the day a flood was recorded in Switzerland obtained with detection scheme IVT_{p85} (left) and anomaly compared to the reference period 1979-2011 (right). Seasonal anomalies were obtained by dividing the frequencies in the left column with the frequencies of the reference period (Appendix Fig. A.5 left). A value of 1 indicates no difference between both frequencies. A value of 2 indicates two times more ARs compared to the reference period. The star indicates the location of Switzerland and N the number of flood days per season.*

The visual analysis clearly showed that all 8 flood events (corresponding to 13 flood days) were caused by ARs bringing moist air from the North Atlantic towards Switzerland in a NW-W flow. In 5 cases (63%) the ARs were observed over Switzerland on the day preceding or the day of the flood, while for 3 cases (37%) ARs were observed over the country 2 to 3 days prior to the event.

Days experiencing winter-time floods in the Jura region (Appendix Fig. A.7) show similar AR frequency patterns and values as those observed for Switzerland, which is easily understandable since this region was affected by all the flood events recorded at that season.

Spring events

On spring flood days, we observe high AR/HIA frequency off the Portuguese coast, over western and central Europe, as well as in the western Mediterranean and Adriatic Seas (up to 95%, Fig. 4.5c). Over Switzerland, 55-75% (IVT_{p95}) to 80-100% (IVT_{p85}) of the cases show AR/HIA conditions on the day preceding or the day of the flood event. The anomaly plot (Fig. 4.5d) shows increased AR/HIA activity over the regions mentioned above compared to the reference period of the order of 2.5 (IVT_{p85}) to 6.5 (IVT_{p95}). Since high frequencies and anomalies are observed both in the eastern North Atlantic and in the Mediterranean Sea, it seems that moisture fluxes towards Switzerland on flood days come from both regions, in SW-NE flows.

Based on the visual analysis, we found that from a total of 12 flood events (corresponding to 18 flood days), 5 events (42%) showed signs of intense moisture transport towards Switzerland on the day preceding or the day of the flood, either in ARs from the WSW (3 events) or in HIAs from the SW-SE (2 events). In addition, for 3 events (25%) AR characteristics were observed over Switzerland 2 to 3 days prior to the event and could have influenced the occurrence of the flood. The remaining events showed either HIAs from the NE related to Vb situations (3 events - 25%) or no AR or HIA characteristics over Switzerland (1 event - 8%). Hence, our observations suggest that 42-67% of the spring-time flood events were related to intense moisture transport towards Switzerland within ARs or HIAs up to 3 days prior to the flood.

Days experiencing spring-time floods in the Jura region (Appendix Fig. A.8) show similar patterns of AR/HIA frequency as those observed for Switzerland, with however higher frequency and anomaly values (AR/HIA frequency reaching 100% for IVT_{p85}). On a total of 8 events, 5 events (63%) showed signs of ARs (3 events) or HIAs (2 events) over Switzerland on the day preceding or the day of the event. For the 3 remaining events (37%), AR characteristics were observed over the country 2 to 3 days prior to the event. Hence, this region seems to be more influenced by intense moisture transport than other regions of Switzerland, with 63-100% of the events being related to ARs or HIAs, which is higher than the proportions found with the visual analysis for Switzerland.

Summer events

On summer flood days, we notice a circular pattern of high AR/HIA frequency over the western Mediterranean and on the southern side of the Alps (up to 85%), however lower AR/HIA frequency is observed over the North Atlantic ($<60\%$, Fig. 4.5e). Over Switzerland, between 35-50% (IVT_{p95}) and 55-75% (IVT_{p85}) of the cases show AR/HIA conditions on the day preceding or the day of the flood event. The anomaly plot (Fig. 4.5f) shows increased AR activity over the southern North Atlantic and western Europe of the order of 1-2 (IVT_{p85}) to 1-2.5 (IVT_{p95}) compared to climatological values. Over the western Mediterranean, anomalies are much higher (up to 5 for IVT_{p95}). Since anomalies over the Mediterranean are higher than over the North Atlantic, it suggests that on flood days most moisture fluxes come from the Mediterranean in a SW-NE flow, while a smaller proportion come from the North Atlantic in a SW flow.

Based on the visual analysis, we found that from a total of 50 flood events (corresponding to 60 flood days), 21 events (42%) showed signs of intense moisture transport towards Switzerland. This transport occurred under different forms; either in ARs arriving in a WSW-SW flow (11 events), in ARs being taken into cyclones and approaching from the SW (5 events) or in HIAs from the SW-S (5 events). In addition, for 7 events (14%) an AR was present over the country 2 to 3 days prior to the flood event and was, in some cases, followed by HIAs from the Mediterranean. However, in these cases the influence of the ARs and HIAs on the occurrence of the flood events is difficult to determine. Finally, for 2 events (4%) we observed HIAs from the NE related to Vb situations and for the remaining 20 events (40%) no AR or HIA characteristics were visible over Switzerland. Hence, our observations suggest that 42-59% of the summer-time flood events were related to the presence of ARs or HIAs situated over Switzerland up to 3 days prior to the flood.

Days experiencing summer-time floods in the Prealps and in Eastern Switzerland (Appendix Fig. A.9a,b,c,d) show similar patterns of AR/HIA frequency and anomalies as those observed for Switzerland, however with higher values for IVT_{p85} (frequency of 45-55%) and lower values for IVT_{p95} (frequency of 15-30%, not shown). With a particularly clear signal of high AR/HIA frequency above Italy (up to 90%), it seems that moisture advection from the Mediterranean in a NE flow (Vb situations) has a relatively high influence on the occurrence of summer flood events in these regions. The visual analysis of single events was not sufficient to support this hypothesis, since from a total of 18 events, only 1 event (5%) showed signs of a HIA from the NE related to a Vb situation, while 8 events (45%) did not show any AR or HIA characteristics. However, since the algorithm does not detect all moisture fluxes related to Vb situations (see Section 4.1), some events for which no AR/HIA characteristics were

observed could have been caused by HIAs related to Vb situations. Furthermore, 6 events (33%) showed AR/HIA characteristics over Switzerland the day or one day before the flood event and 3 events (17%) showed similar signs 2 or 3 days prior to the event.

Days experiencing summer-time floods in the Ticino region (Appendix Fig. A.9e,f) also show similar patterns of AR/HIA frequency as those described for Switzerland, with however higher frequency and anomaly values. In particular, especially high values are observed over the western Mediterranean and southern Alps (frequency of 70-100% for IVT_{p85}). From a total of 17 events, 11 events (64%) showed signs of AR (7 events) or HIA (4 events) characteristics over Switzerland on the day preceding or the day of the flood and for 3 events (18%) AR characteristics were observed over the county 2 to 3 days prior to the event. Finally, for 1 event (6%) we observed a HIA from the NE related to a Vb situation and the last 2 events (12%) did not show any AR or HIA characteristics.

Fall events

On fall flood days, we observe high AR frequency southwest of the Iberian Peninsula (up to 60%, Fig. 4.5g), as well as over central Europe and the western Mediterranean (up to 90%). Over Switzerland, between 50-85% (IVT_{p95}) and 60-90% (IVT_{p85}) of the cases show AR conditions on the day preceding or the day of the flood event. The anomaly plot (Fig. 4.5h) shows anomalies of 1.25-2 (IVT_{p85}) and 2-3 (IVT_{p95}) over the eastern North Atlantic, while higher anomalies (2-3 for IVT_{p85} and 2.5-6.5 for IVT_{p95}) are observed over the western Mediterranean and central Europe, in particular on the southern side of the Alps. As for summer, this suggests that on fall-time flood days, moisture fluxes from the western Mediterranean in SW-NE flows have a particularly high influence on the occurrence of flood events, especially on the southern side of the Alps. In contrast, moisture fluxes from the North Atlantic in a SW flow have a less importance.

Based on the visual analysis, we found that from a total of 25 flood events (corresponding to 29 flood days), 22 events (88%) showed signs of high moisture transport towards Switzerland the day or one day before the flood. This transport occurred under different forms; either in ARs arriving in a W-SW flow (17 events), in ARs from the NW (1 event) and in HIAs from the south (4 events). In addition, 1 event (4%) showed a HIA from the east related to a Vb situation. For the remaining 2 events (8%), no signs of ARs or HIAs near Switzerland were detected. Hence, our observations suggest that 88% of the fall-time flood events were related to the presence of ARs or HIAs over Switzerland on the day preceding or the day of the flood. We also observed that while most of the ARs seemed to come directly from the North Atlantic in a W-SW flow, 6 of them seemed to be forced southwards over the Mediterranean

Sea before turning northwards towards Switzerland, allowing them to increase their moisture content before being lifted over the Alps.

Days experiencing fall-time floods in the Ticino region (Appendix Fig. A.10) show similar patterns of AR frequency as those observed for Switzerland, however with higher values (95-100% for IVT_{p85}). On a total of 14 events, 13 events (93%) showed signs of ARs (11 events) and HIAs (2 events) over Switzerland on the day preceding or the day of the flood. Out of the 11 ARs, we observed that 4 ARs seemed to be pushed southwards over the Mediterranean Sea before turning northwards towards Switzerland. For the remaining event (7%), no AR/HIA characteristics were observed over the country.

4.3.2.3 Comparison of detected and observed frequencies

Table 4.4 summarizes the frequency of ARs/HIAs over Switzerland detected by the algorithm (detected frequencies) and obtained by subjective verification (subjective frequency) on the day preceding or the day of a flood that were presented in the previous section. One should note that both frequencies are not exactly comparable, since detected frequencies are based on flood days, while the subjective frequency is based on flood events.

The frequency of ARs/HIAs detected by IVT_{p95} for the different seasons shows more or less similar values as those found with the subjective verification. In contrast, IVT_{p85} detects higher AR/HIA frequency in spring and summer. The subjective verification of individual events allowed us to understand this difference; we noticed that IVT_{p85} detects more HIAs from the NE related to Vb situations than IVT_{p95}. Since Vb situations occur rather during the warm season, this results in higher frequencies detected at those seasons.

	Winter	Spring	Summer	Fall
Detected freq. IVT_{p95}	80-100%	55-75%	35-50%	50-85%
Detected freq. IVT_{p85}	90-100%	80-100%	55-75%	60-90%
Subjective frequency	**63-100%**	**42-67%**	**42-59%**	**88%**

Table 4.4: *Seasonal AR/HIA frequency over Switzerland detected by the algorithm (detected frequencies) and obtained by subjective verification (subjective frequency) for the day or one day before a flood. Based on the values and observations presented in Section 4.3.2.2.*

4.3.2.4 Composite plots of flood-related atmospheric rivers

Finally, to gain insight on the synoptic situations responsible for AR activity above Switzerland on the day preceding or day of a flood event, we analyzed seasonal composite plots of sea-level pressure, geopotential height, equivalent potential temperature (θ_e) and potential vorticity (PV). Since we observed with the subjective analysis that HIAs approach Switzerland from a different flow direction than ARs, we suppose that ARs and HIAs are related to different synoptic situations and these plots were only made for AR cases related to flood events in any region of Switzerland and not for HIAs. The method applied to obtain these seasonal composite plots is presented in Section 3.3.2 and the plots are presented in Fig. 4.6. In addition, Fig. 4.7 illustrates typical cases of ARs related to flood events in Switzerland for each season.

In winter, we see that flood-related ARs are associated with a strong pressure gradient over western Europe (Fig.4.6a). We observe a deep low pressure system over Scandinavia, a high pressure system over northern Africa and Spain and a PV ridge over western Europe (Fig. 4.6c), causing the air to flow in a WNW-W flow. The θ_e composite does not show a clear signal (Fig. 4.6b), but we notice warmer air coming from the western tropical Atlantic towards Europe, which brings moist tropical air towards the lower end of the AR tracks observed in Fig. 4.5a. However, this source probably does not contribute to the flood events, since it is located too far away from Switzerland on the day preceding or the day of the event.

In spring, since only three AR events were observed, composite plots do not show a clear signal. Nevertheless, we notice that flood-related ARs are associated with a weak pressure gradient over the North Atlantic (Fig. 4.6d). A weak low pressure system is observed west of the British Isles, as well as a PV ridge over western Europe (Fig. 4.6f), forcing the air to flow towards Switzerland in a W-SW flow. The θ_e composite (Fig. 4.6e) does not show a clear signal, but we notice warmer air coming from the tropics towards Europe in the eastern Atlantic and over northern Africa.

In summer, flood-related ARs are also associated with a weak pressure gradient (Fig. 4.6g). A weak high pressure system is observed over the Azores, extending up to the 55th parallel north in the central Atlantic, while a weak low pressure system is located over the North Sea, forcing the air in a NW flow towards Spain and France. A PV trough over western France associated with lower θ_e (Fig. 4.6h,i) forces the air northwards, resulting in a SW flow towards Switzerland and eastern Europe.

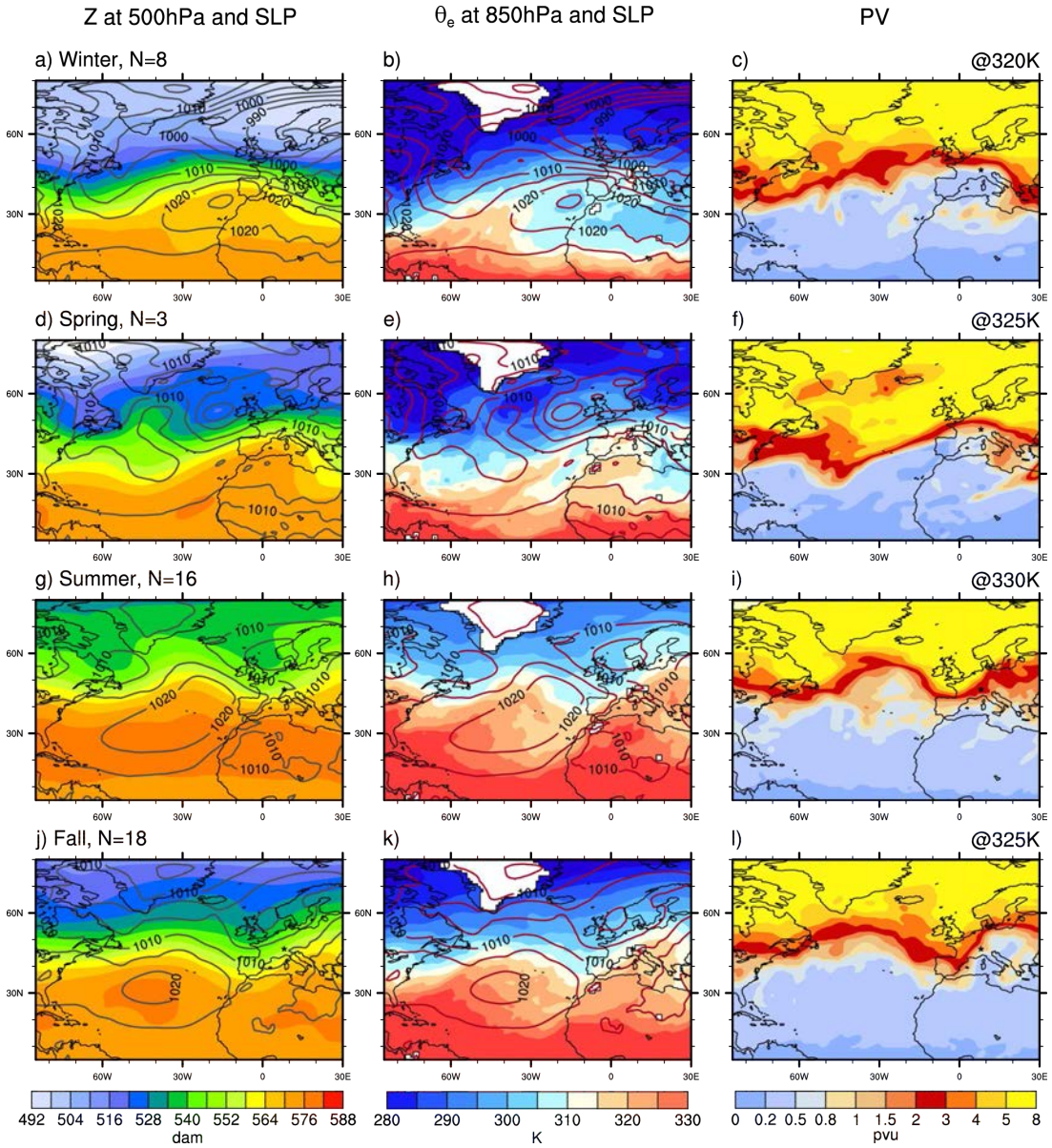

Figure 4.6: *The left plots show the seasonal composite of geopotential height at 500 hPa (Z [dam], in color) and sea level pressure (SLP [hPa], contour lines) for flood events for which ARs were visually identified over Switzerland. The center plots show the seasonal composite of equivalent potential temperature at 850 hPa (θ_e [K], in color) and sea level pressure (SLP [hPa], contour lines) for the same events. The right plots show the seasonal composite of potential vorticity at different isentropic levels (PV [pvu]) for the same events. The star indicates the location of Switzerland and N the number of events used to make the composite. When an event was composed of successive flood days, the date of the event was represented by the date of the first day experiencing flooding in any region of Switzerland.*

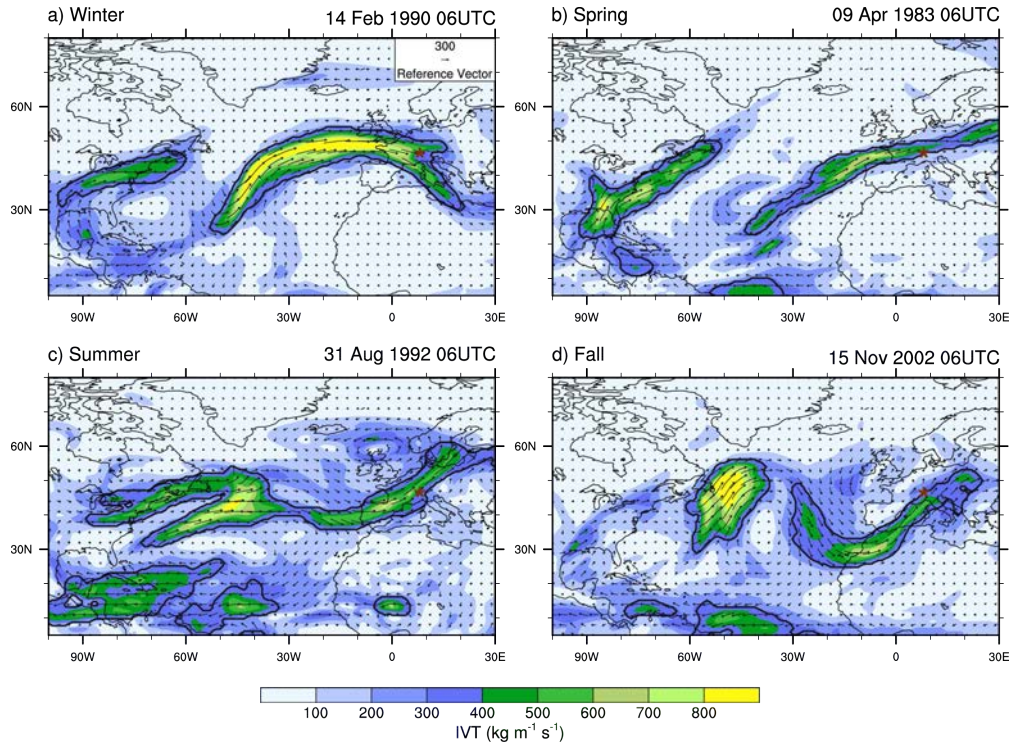

Figure 4.7: *Typical cases of ARs related to floods in Switzerland for each season. Colors and overlaid vectors represent the IVT and the direction of transport. ARs detected with scheme* IVT_{350} *are represented in black contour. The brown star indicates the location of Switzerland.*

Finally in fall, flood-related ARs are associated with a high pressure system over the southern North Atlantic and a low pressure system over Scandinavia, extending south towards central and western Europe and forcing the air in a NW flow (Fig. 4.6j). As for summer, a PV trough (Fig. 4.6l) associated with lower θ_e over western France (Fig. 4.6k) could explain why the air is forced northwards over this region, resulting in a SW flow over Switzerland and central Europe. Depending on the position of the PV trough, in some cases the ARs pass over the Mediterranean Sea before turning northwards towards the continent.

4.4 Relation between atmospheric rivers and extratropical cyclones

Finally, the algorithm output also allowed us to analyze the relation between ARs and extratropical cyclones. This was done through the analysis of a case study of the winter season December 1989 to February 1990. During this season, 27 different AR events were

observed over the North Atlantic Ocean, which seemed to be related to moisture plumes from the Caribeean Sea and from the western or central tropical North Atlantic. In addition, 4 HIAs were observed over the Mediterranean and North Africa, which seemed to be related to moisture plumes from the eastern tropical Atlantic. For each of these events, the relation with fronts (Section 4.4.1) and WCBs (4.4.2) was analyzed and the results are presented in the following sections.

4.4.1 Atmospheric rivers and fronts

To investigate the relation between ARs/HIAs and fronts, we first performed an overlap of ARs and frontal patterns (see Section 3.4.1 for the method description). Then, the overlapping ARs and fronts were plotted, as well as non-overlapping fronts, in order to evaluate the overlapping method. We noticed that in some cases, frontal patterns that were separated by a few grid points from an AR were not considered as overlapping at certain time steps, while they were found to overlap at other time steps. This concerned especially warm fronts located at the head of ARs, but also frontal structures on the northwestern flank of ARs. Two examples of cold and warm fronts not overlapping the detected ARs at a given time step are presented in Fig. 4.8. However, AR structures were not affected by this effect, since they are big and were often observed to overlap several frontal patterns. Hence, from the case study it seems that the method can be used to detect front-related ARs/HIAs, however, frontal patterns should be slightly enlarged in order to detect all fronts overlapping AR/HIA structures.

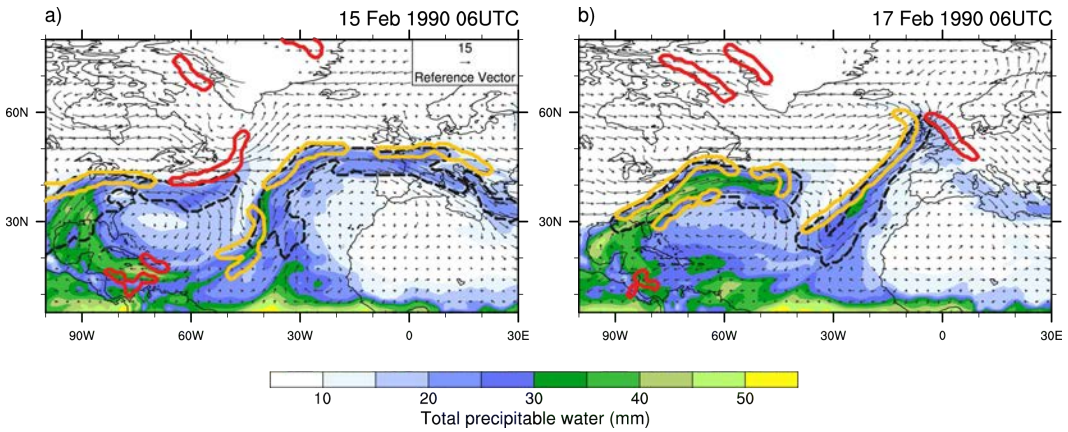

Figure 4.8: *Example of time steps for which fronts related to ARs do not overlap the AR structures, with TPW (in color), wind speed at 750 hPa (arrows), ARs detected with the TPW_{20} scheme (dashed black contour), fronts overlapping with ARs (orange contour) and fronts not overlapping with ARs (red contour).*

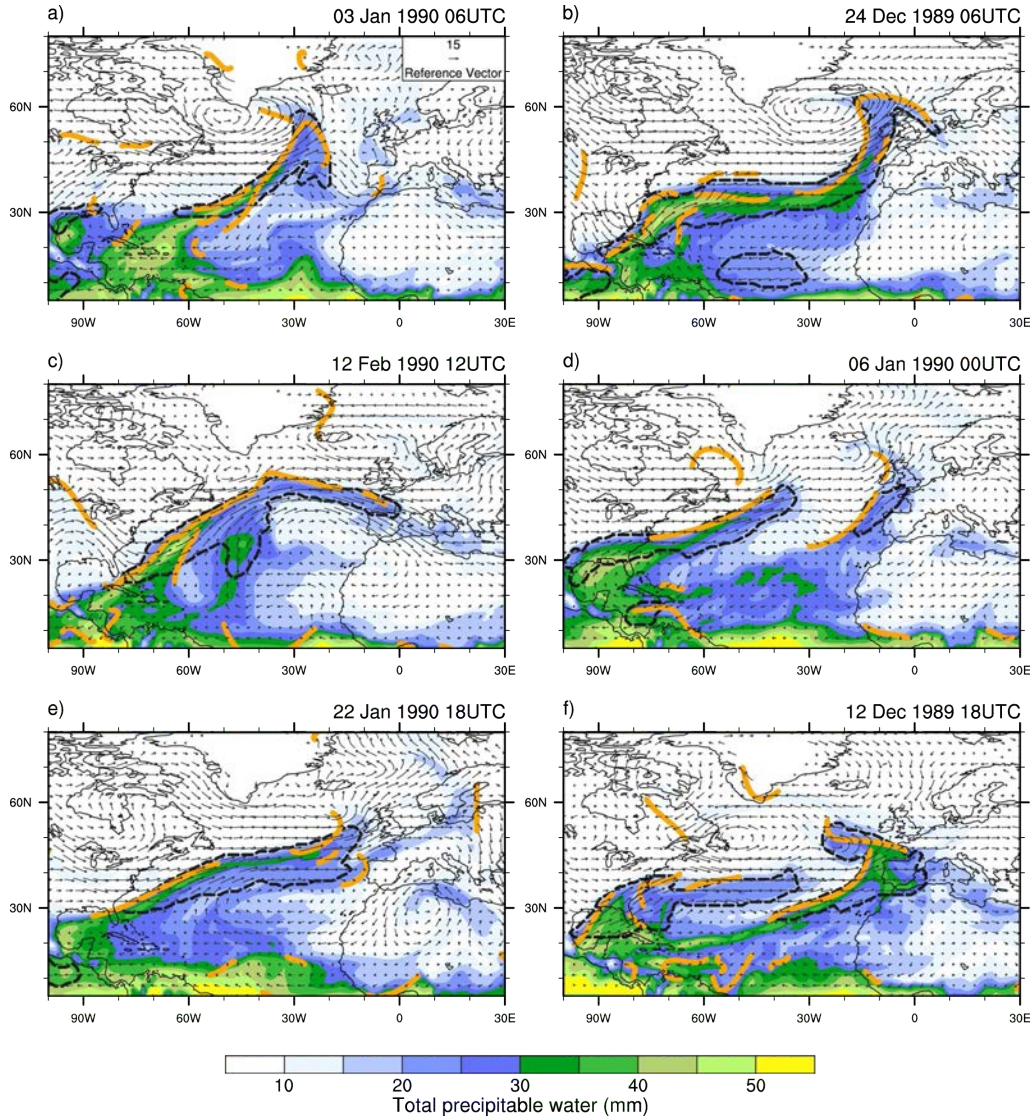

Figure 4.9: *Examples of AR cases for the winter season December 1989 to February 1990, with TPW (in color), wind speed at 750 hPa (arrows), ARs detected with the TPW_{20} scheme (dashed black contour) and frontal lines (in orange). Frontal lines are based on a spline interpolation of the front data, courtesy of S. Schemm.*

In a second step, the plots were analyzed, in order to investigate the relation between the ARs/HIAs and the fronts. As mentioned above, during the winter 1989-1990, we observed 27 ARs over the North Atlantic Ocean and 4 HIAs over the Mediterranean and North Africa. Fig. 4.9 illustrates six examples of ARs, while the four HIA cases are presented in the appendix (Fig. A.11). For most ARs, we observed frontal structures overlapping the northwestern flank of the ARs. For HIAs, no frontal structures were observed with the front data used for the study. However, when creating the plots presented in this section, we used the front data produced with the more recent version of the front detection algorithm (see Section 2.3) and

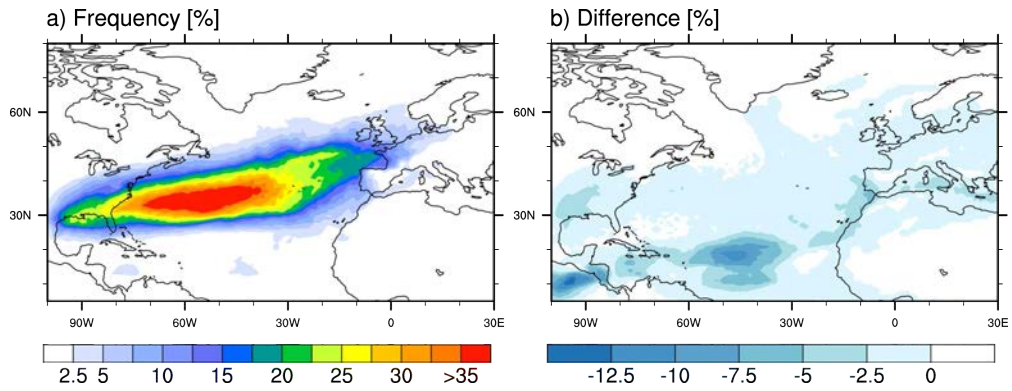

Figure 4.10: *a) Seasonal frequency of ARs/HIAs overlapping with fronts for the winter 1989-1990 obtained with detection scheme TPW_{20} and b) difference compared to the frequency of all ARs for the same time period obtained with the same detection scheme. The difference plot was obtained by subtracting the overlapping frequency by the frequency of all ARs for the same time period.*

noticed that one HIA showed a small front overlapping the northwestern flank of its tail (Fig. A.11d). In addition, for another HIA a front was observed close to the tail (Fig. A.11c).

The majority of the AR events (24 ARs) showed signs of the presence of forming or developed extratropical cyclones at the head or at the center of the ARs, with cold and warm fronts clearly visible, as well as cyclonically turning winds (Fig. 4.9a,b,c). Only 3 events did not show a clear relation with extratropical cyclones. Two events showed ARs forming in the warm sector of a small extratropical cyclone over the eastern U.S., with developed cold and warm fronts. However, the cyclone seemed to dissipate over the continent and the AR was then taken in the westerly flow south of a cyclonic system, with frontal structures on its northwestern flank (Fig. 4.9d(left),e). The last event showed an AR forming in the strong westerly flow south of a cyclonic system, catching up with the preceding AR (Fig. 4.9f(left)). Even though frontal structures were observed on its northwestern flank, they could not be related to the frontal patterns of an extratropical cyclone.

Furthermore, we observed that some ARs were related to several cyclonic systems. Indeed, 12 cases showed secondary extratropical cyclones forming in the tail of the ARs, with the related cold and warm fronts (e.g. Fig. 4.9b). In some cases, these cyclones reinforced the preexisting AR, while in other cases they formed a new and distinct AR.

Our findings about the strong relation between ARs and fronts are supported by the analysis of the frequency plots presented in Fig. 4.10, which show the frequency of ARs/HIAs overlapping with fronts for the winter 1989-1990 over the North Atlantic and the difference

compared to the frequency of all ARs for the same time period. We observe that both frequency values are very similar, with differences of 0 to -2.5% over the North Atlantic and 0 to -5% on the coast of Morocco and in the Mediterranean Sea. Since we observed that most ARs overlap with frontal patterns over the North Atlantic, this results in a high proportion of front-related ARs detected by the overlap method and to small frequency differences. Over the eastern North Atlantic and Mediterranean Sea, we observed HIAs which did not overlap with frontal patterns, which explains why frequency differences are larger over these regions.

4.4.2 Atmospheric rivers and warm conveyor belts

To investigate the relation between ARs/HIAs and WCBs, plots of ARs, fronts and WCBs for the winter season 1989-1990 were created. While all 4 HIA events showed no relation with WCBs, we found that all 27 ARs seemed to be linked to preascending and ascending WCBs. Most cases (23 events) showed preascending and ascending WCBs overlapping with ARs in the early stages of formation of the ARs over the Caribbean Sea and western Atlantic. They were mostly observed on the sides of the ARs (preascending WCBs) and at the head or in the middle of the ARs (ascending WCBs). The ascending WCBs were related to extratropical cyclones with developed frontal systems as described in Section 4.4.1. The remaining 4 cases showed WCBs appearing in later stages either in the head or in the center of the ARs, along with the formation of developing extratropical cyclones. In addition, some ARs showed overlapping with several WCB patterns. For example, all the ARs for which we observed secondary extratropical cyclones forming in their tail (see Section 4.4.1) also showed secondary WCB patterns in their tail.

As an example, Fig. 4.11 illustrates the evolution of an AR and the related WCBs for 23 to 25 December 1989. We see an AR originating in the western tropical Atlantic, with an ascending WCB at its head, associated with an extratropical cyclone (visible with cyclonically turning winds) and a frontal system (Fig. 4.11a). Preascending WCBs are also observed in the central and eastern North Atlantic close to the AR. The AR evolves over the North Atlantic, together with the cyclone and the WCB (Fig. 4.11b,c). On 24 December at 12 UTC (Fig. 4.11d), we observe that the WCB is taken into the cyclonic rotation of the extratropical cyclone, which leads to the dissipation of the AR shortly after (Fig. 4.11e,f). At the same time, we also notice the apparition of a secondary WCB in the tail of the AR (Fig. 4.11b). This WCB is associated with a developing extratropical cyclone, which shows a few time steps later a developed frontal system (Fig. 4.11e). This secondary cyclone constitutes a new AR on 26 December, when the leading end of the AR described above dissipates (not shown).

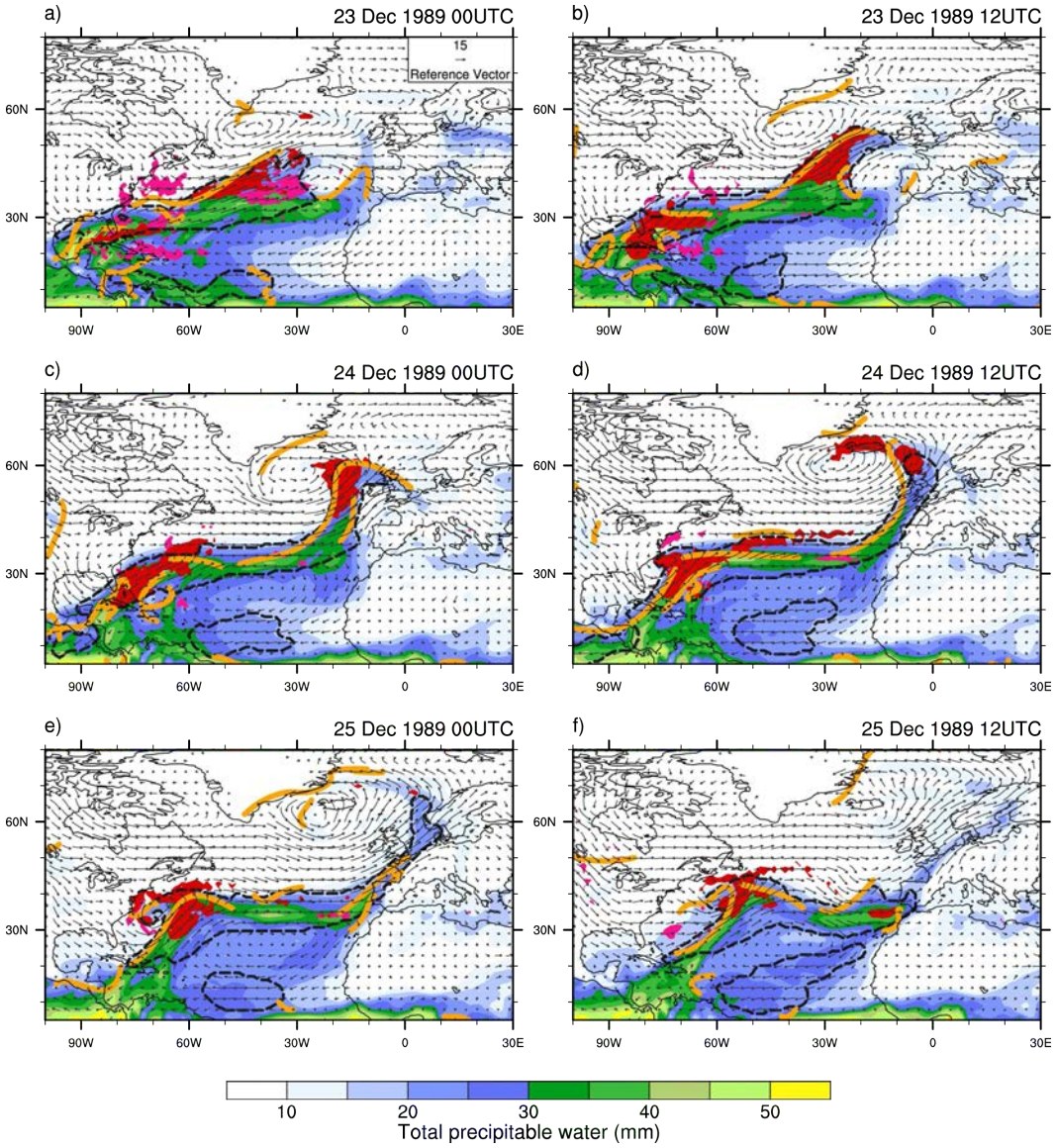

Figure 4.11: *Example of an AR and its relation with preascending and ascending WCBs for the time period 23-25 December 1989, with TPW (in color), wind speed at 750 hPa (arrows), ARs detected with the TPW_{20} scheme (dashed black contour), frontal lines (in orange), preascending WCBs (in pink) and ascending WCBs (in red). WCBs are given in units of WCBs per km^2 and contours include all densities larger than 0.0002 WCBs/km^2. Frontal lines are based on a spline interpolation of the front data, courtesy of S. Schemm.*

While this example illustrates the dissipation of an AR after the related WCB is taken in the cyclonic flow, we noticed that in other cases, ARs became decoupled from the WCBs and did not dissipate. An example of such a case is illustrated in Fig. 4.12 for 18 to 20 February 1990. An AR is visible over the North Atlantic on 18 February 1990 (Fig.4.12a), which is related to a developing extratropical cyclone (visible on Fig. 4.12b with cyclonically turning winds). This cyclone is associated with a frontal system and a WCB. On

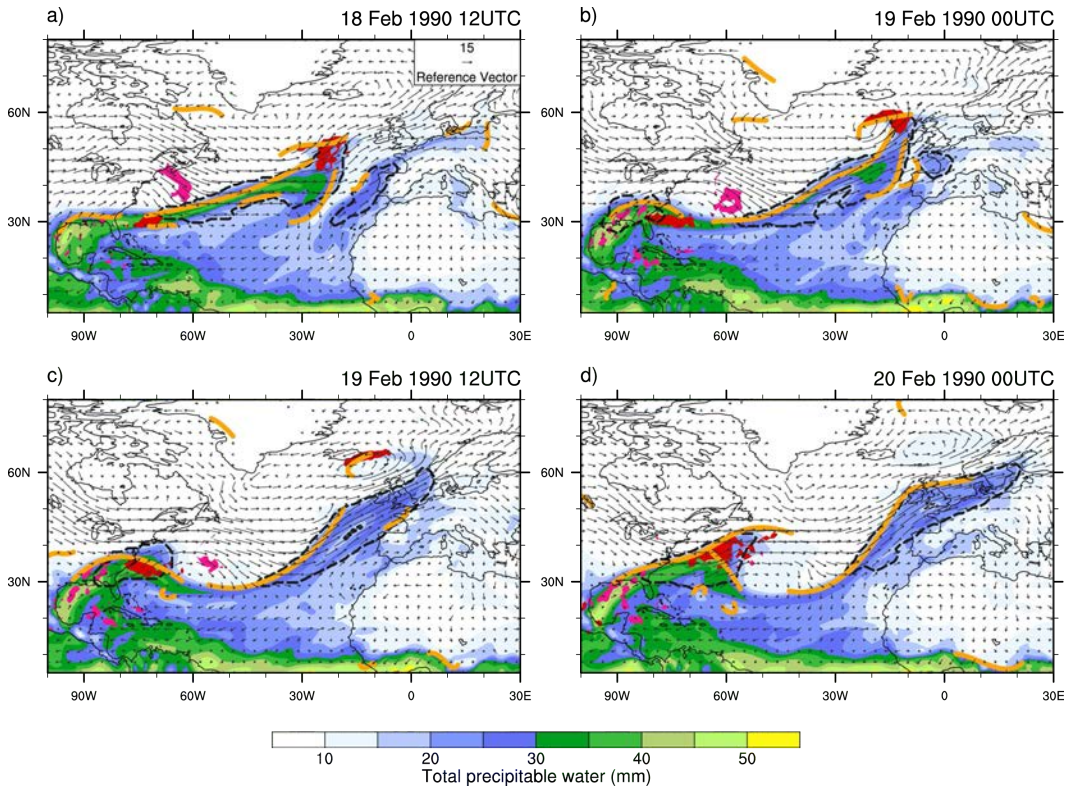

Figure 4.12: *Same as Fig. 4.11 but for the time period 18-20 February 1990.*

19 February at 00 UTC (Fig. 4.12b), we see that the WCB is being taken into the cyclonic rotation of the extratropical cyclone. However, in this case the AR persists in the next time steps and continues to flow northeastwards in the westerly flow south of the associated cyclone (Fig. 4.12c,d). In addition, we notice in Fig. 4.12c,d a developed frontal system along the northwestern flank of the AR, as well as a distortion in the wind field, suggesting the presence of a secondary developing extratropical cyclone.

These two examples suggest that ARs and WCBs are closely related over the western North Atlantic, but can exhibit different behaviors over the eastern North Atlantic, where in some cases they seem to become decoupled. On the 27 ARs observed during this winter season, we found that 9 cases showed ARs dissipating shortly after the related WCB was taken in the cyclonic rotation of the cyclone (similar to the case of 23-25 December), while 18 cases showed ARs becoming decoupled from the WCBs and continuing their path eastwards in the westerly flow south of the extratropical cyclones to which they were previously associated (similar to the case of 18-20 February).

Therefore, it seems that over the western North Atlantic, most of the ARs/HIAs are related to WCBs, while this relation decreases eastwards. These findings are supported by the analysis of the frequency plots presented in Fig. 4.13, which show the frequency of

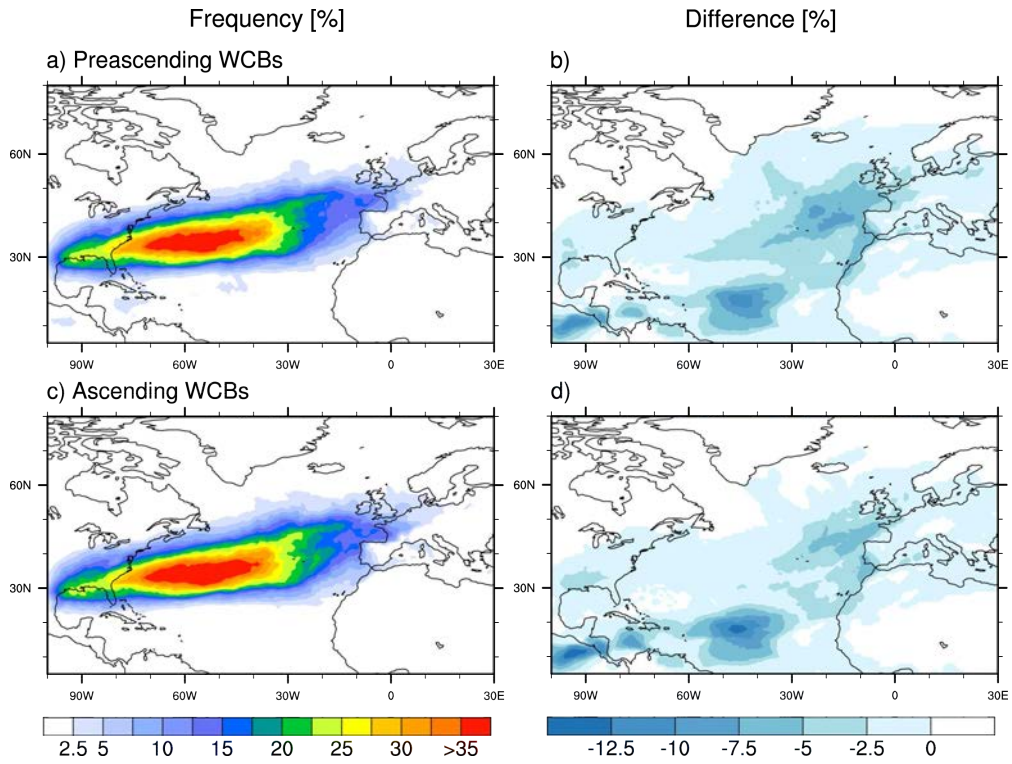

Figure 4.13: *Seasonal frequency of ARs/HIAs overlapping with preascending and ascending WCBs for the winter 1989-1990 obtained with detection scheme TPW_{20} (left) and difference compared to the frequency of all ARs for the same time period obtained with the same detection scheme (right). The difference plots were obtained by subtracting the overlapping frequency by the frequency of all ARs for the same time period.*

ARs/HIAs overlapping with preascending and ascending WCBs for the winter 1989-1990 and the differences compared to the frequency of all ARs/HIAs for the same time period (see Section 3.4.2 for the method description). Over the western North Atlantic, frequency values of ARs/HIAs overlapping with WCBs are very similar to those of all ARs, with a maximum frequency of 40% and differences between 0 and -5%. However, over the eastern North Atlantic, the frequency of ARs/HIAs overlapping with WCBs is 5-7.5% lower than for all ARs, with frequency values of 10-22.5% for ARs/HIAs overlapping with preascending WCBs (Fig. 4.13a) and 12.5-25% for ARs/HIAs overlapping with ascending WCBs (Fig. 4.13c). Furthermore, we notice that the relation between ARs/HIAs and ascending WCBs seems to be slightly stronger than between ARs/HIAs and preascending WCBs, the latter showing more pronounced frequency differences, especially over the eastern North Atlantic. With the visual analysis, we noted that preascending WCBs are mostly present on the sides of the ARs, thus showing less overlap, and that they are more rare over the eastern North Atlantic, which explains why the overlapping frequencies are lower over that region than for ascending WCBs.

Chapter 5

Discussion

In this chapter, the results presented in the previous chapter are discussed. First, the AR detection algorithm is evaluated and its limitations are noted (Section 5.1). Then, the AR climatology obtained with different detection schemes is compared to findings from other studies (5.2). Next, we explain the seasonal and regional influences of ARs/HIAs on flood events that were observed in Switzerland (5.3). Finally, we discuss findings concerning the relation between ARs, fronts and WCBs (5.4).

5.1 Atmospheric river detection algorithm

The AR detection algorithm consisted of four different detection schemes, which used criteria to detect ARs which were inspired from the literature (Ralph et al., 2004; Neiman et al., 2008b; Lavers et al., 2011; Ralph and Dettinger, 2011). It could be run in a relatively short time span and allowed the detection of AR characteristics over a particular region at a given time step. We found that not only did it detect ARs as defined by the literature (i.e. long and narrow corridors of intense moisture transport, Lavers and Villarini, 2013), but it also detected structures having similar characteristics as ARs but a shorter length ($< 2000\,\mathrm{km}$) that we named HIAs (high IVT areas). This was allowed by the use of a simple size criterion only, discriminating features smaller than ca. $263{,}000\,\mathrm{km}^2$ in the mid-latitudes (i.e. 30 grid cells). Since HIAs can bring considerable amounts of moisture towards the land and can participate to the triggering of heavy precipitation and flood events, they are also of interest when studying moisture fluxes towards the continent.

However, we also noticed that the algorithm had several limitations. First of all, we observed that the schemes based on the IVT detected structures in the tropics that were not detected by the scheme based on the TPW and wind speed. They are probably convection structures and their detection is related to the definition of the IVT. The latter is calculated by integrating the combination of the specific humidity and of the wind speed. When convection occurs, the specific humidity is increased, thus increasing the IVT, resulting in high IVT values even in cases where the wind speed is low. Since our research focused on the North Atlantic Ocean domain and was not affected by this effect, no correction was applied. However, such a correction could be made, for example, by removing all patterns that do not have at least one grid point north of 25°N.

A second limitation was the low ability of some detection schemes to detect ARs/HIAs over land. Because of the moisture depletion of air masses as they travel over land, the TPW and IVT values decrease with distance from the sea and can quickly reach values lower than the thresholds set in the fixed-threshold-based detection schemes (TPW_{20} and IVT_{350}). This leads to the low detection of AR/HIA patterns over land, even though in some cases the moisture fluxes are significantly different from normal conditions. For this reason, detection schemes TPW_{20} and IVT_{350} could not be used to study ARs/HIAs over Europe and their influence on Swiss flood events, but were replaced by percentile-based detection schemes (IVT_{p85} and IVT_{p95}). The latter evaluate moisture fluxes compared to local percentile values and thus take into account the fact that the IVT value of significant moisture fluxes can vary considerably between regions according to their climate conditions. This underlines the fact that no perfect detection scheme exists and that depending on the focus of the study, different schemes are preferred.

A third limitation arose from the observation made in Section 4.3.1, where we noticed that the algorithm detected some, but not all, HIA patterns related to Vb situations. Indeed, in many cases the areas having HIA characteristics (i.e. TPW or IVT above the thresholds fixed by the detection schemes) were often smaller than the 30 grid cells defined by the size criterion and thus the patterns were not detected by the algorithm. However, regardless of their small size, these structures sometimes bring large amounts of moisture towards the land and can cause floods.

Nevertheless, despite these limitations, the algorithm was found to detect well ARs and HIAs and the algorithm output was used to compute the seasonal climatological frequency of ARs/HIAs, to investigate the influence of ARs/HIAs on flood events in Switzerland, as well as to investigate the relation between ARs/HIAs, fronts and WCBs.

5.2 Atmospheric river climatology

The seasonal climatological frequency of ARs/HIAs obtained with detection schemes TPW_{20} and IVT_{350} (Section 4.2) showed higher AR/HIA frequency over the eastern North Atlantic and Europe in summer and fall, while lower activity was observed in winter and spring. In contrast, in Section 4.3.2.2 we observed that percentile-based detection schemes IVT_{p85} and IVT_{p95} showed higher AR/HIA frequency in winter and fall compared to summer over the North Atlantic. Therefore, depending on the detection schemes, the frequency maximum of ARs/HIAs was observed at different seasons. These differences are related to the fact that fixed-threshold based detection schemes are sensitive to changes in the moisture content of the air with the season, while percentile-based schemes are not affected by this effect. Through the Clausius-Clapeyron relation, we know that an increase in temperature leads to an increase in the saturated vapor pressure of the air (Wallace and Hobbs, 2006). Since during the warm season temperatures are higher, the air also holds more moisture. Consequently, TPW and IVT values more often exceed the detection thresholds fixed by the schemes and more AR/HIA patterns are detected than during the cold season. In contrast, percentile-based schemes, which detect moisture fluxes occurring a certain percentage of the time, have detection thresholds which vary with the month. Consequently, less AR/HIA structures are detected by these schemes in summer compared to fixed-threshold-based schemes.

According to the literature, ARs are more frequent during the cold season. At that season, the westerly circulation is stronger due to a stronger latitudinal temperature gradient. This produces a strong baroclinic zone, leading to an increased number of extratropical cyclones crossing the Atlantic (Lavers and Villarini, 2013). Since ARs are closely related to extratropical cyclones (Ralph et al., 2004, 2005; Bao et al., 2006; Ralph and Dettinger, 2011), this leads to a higher probability of AR occurrence. In summer, the temperature gradient and the westerly circulation are weaker, with also fewer extratropical cyclones reaching Europe, leading to a lower probability of AR occurrence (Lavers and Villarini, 2013). Similar findings were observed in this study with detection schemes IVT_{p85} and IVT_{p95}, where higher AR/HIA frequency was observed in winter and fall. However, one should note that while most studies focused on ARs defined as corridors of intense moisture transport with a length of $>$ 1500-2000 km (e.g. Lavers and Villarini, 2013; Rutz et al., 2014), we also considered smaller structures (HIAs). Since we observed that HIAs especially occur in summer and in fall (Section 4.3), considering them in the climatology of ARs leads to higher detected frequencies during these seasons compared to a climatology which would be solely based on ARs. This is particularly the case for the Mediterranean Sea where many HIAs were observed. However, as far as the author knows, no such climatology exists, hence no comparison is possible.

Concerning the spatial patterns of the AR/HIA frequency maxima, we found that the patterns observed in the AR/HIA climatology resemble those of the storm tracks climatology (Hoskins and Hodges, 2002). This is not surprising, since we know from the literature that most ARs occur in the warm sector of extratropical cyclones and evolve with the mid-latitude storm track (Ralph et al., 2004, 2005; Bao et al., 2006; Ralph and Dettinger, 2011). In addition, we observed that the orientation of the AR/HIA frequency maxima vary according to the season. In summer and fall, ARs/HIAs seem to be rather zonally oriented over the North Atlantic, while they have a more SW-NE orientation in winter and spring. These findings are in agreement with previous studies of ARs in the North Pacific, which showed that winter-time ARs form in the tropical eastern Pacific Ocean and cross the ocean in a SW-NE direction, while summer-time ARs originate in extratropical regions and are more zonally oriented (Neiman et al., 2008b; Knippertz et al., 2013). While these findings suggest that the moisture source of ARs varies with the season, situated in the tropics during the cold season and in the extratropics during the warm season, other studies have shown that even though winter-time ARs seem to originate in the tropics, the direct transport of moisture from the tropics to the extratropics in a river-like way is not always observed (Bao et al., 2006; Neiman et al., 2013). Indeed, it was found that most cases rather show ARs forming through local moisture convergence within extratropical cyclones, suggesting that even during the cold season, the moisture transported in ARs does not always have a tropical origin (Bao et al., 2006).

5.3 Relation between atmospheric rivers and floods in Switzerland

The climatology of ARs/HIAs presented in Section 4.2 that was obtained with detection schemes TPW_{20} and IVT_{350} suggested that ARs/HIAs occur over Switzerland 2.5 to 7.5% of the time depending on the season and thus are quite rare. Since these fixed-threshold-based schemes showed limited detection over land, percentile-based schemes were preferred to study the influence of ARs/HIAs on flood events in Switzerland, showing better detection over land (Section 4.1). These schemes detect an AR when the magnitude of a moisture flux over a given grid point exceeds the IVT value which occurs 15% (IVT_{p85}) and 5% (IVT_{p95}) of the time. Hence, they detect fluxes having lower magnitude than those detected by TPW_{20} and IVT_{350} and thus more frequent fluxes. In addition, by considering all moisture fluxes occurring 48 hours prior to a given date, more or larger ARs/HIAs are detected. When comparing detected frequencies with frequencies obtained by subjective verification, we noticed that

detection scheme IVT_{p95} showed small differences between detected and subjective frequencies (Section 4.3.2.3). In contrast, IVT_{p85} showed higher detection in spring and summer. This difference is due to the fact that the latter detects more HIAs related to Vb situations than IVT_{p95}, which are prevalent during the warm season. However, one should also note that both frequencies are not exactly comparable, since detected frequencies are based on flood days, while the subjective frequencies are based on flood events (as defined in Section 3.3.2). Hence, if consecutive days record floods in one region, the influence of that event is multiplied by the number of days it lasted, which can lead to an over-estimation of detected frequencies. On a total of 95 flood events, 20 events lasted more than one day and almost half of them (8 events) occurred during the summer, which can also explain why detected frequencies at that season are larger than the frequency obtained with the subjective verification.

The analysis of flood events in Switzerland showed that ARs and HIAs have different seasonal and regional influences on floods. In winter, for most floods we observed ARs over Switzerland up to 3 days prior to the events, flowing in a NW-W flow. The Jura, which recorded most winter-time floods, was the region the most affected by the ARs, with all of the events showing AR conditions. In spring, for 42-67% of the floods we observed ARs or HIAs above the country up to 3 days prior to the events, flowing respectively in a WSW and SW-SE flow. At that season, we found that the Jura is particularly sensitive to these intense moisture fluxes, with a higher proportion of flood events showing AR/HIA conditions (62-100%) compared to Switzerland as a whole. In contrast, Eastern Switzerland, for which no analysis was provided but which also measured a high proportion of floods at that season (Table 4.3), was found to be more affected by HIAs from the NE related to Vb situations (50%) rather than by ARs/HIAs (only 33%). In summer, 42-59% of the floods showed AR/HIA conditions over the country up to 3 days prior to the events, with ARs arriving in a WSW-SW flow and HIAs flowing in a SW-S flow. We found that Ticino is the region the most affected by ARs/HIAs, since they were observed for 64-82% of the flood events, against only 33-50% for the Prealps and Eastern Switzerland. Finally, for 88% of the fall-time floods ARs/HIAs were observed over Switzerland on the day preceding or the day of the event, arriving respectively in a W-SW and southerly flow. One exception was noted, the AR of 10 October 2011, which arrived from the NW. At that season, Ticino is particularly sensitive to ARs/HIAs, 93% of the floods showing AR/HIA conditions.

Hence, according to these findings, ARs and HIAs particularly affect floods during the cold season (winter and fall), and to a smaller extent in spring and summer. These findings are in agreement with the research of Lavers and Villarini (2013), who found that annual maxima precipitation were mostly influence by ARs in winter and fall. They explain this by an increased AR activity during the cold season, due to an increased extratropical cyclone

activity at that season, as mentioned in Section 5.2. In addition, Neiman et al. (2008b) found that cold-season ARs have more impacts on coastal precipitation than warm-season AR. For them, despite the air having low saturated vapor pressure in the cold winter air, the vapor transport at that season is stronger than in summer due to stronger storms, which cause stronger flows.

Furthermore, the air being close to saturation in winter, rain can occur more easily (Neiman et al., 2008b), especially in the case of orographic lifting in mountainous regions, where topography plays an essential role as a lifting process for the triggering of heavy precipitation (Lavers and Villarini, 2013). In complex topographies, the direction of the flow also influences the regions affected by heavy precipitation and floods, depending on the topography, basin orientation and rain shadowing (Neiman et al., 2011). In Switzerland, Schmocker-Fackel and Naef (2010) found that floods in the Jura and Plateau are related to westerly flows (NW-SW), while floods in the central part of Switzerland are related to NE flows. On the southern side of the Alps, floods are produced by southerly flows (SW-S) and the lifting of the air over the Alps (Massacand et al., 1998; Schmocker-Fackel and Naef, 2010). Our study showed that ARs/HIAs related to winter and spring-time floods came from a westerly direction. Considering the findings of Schmocker-Fackel and Naef (2010), we understand why these flows generated mostly floods in the Jura region. Similar conclusions can be drawn for the Ticino region in fall and summer. Therefore, the topography and the flow direction are both factors which contribute to the observed seasonal and regional disparities of AR/HIA influence on floods in Switzerland.

While the analysis provided interesting results, some uncertainties remain. For example, to what extent the ARs observed over Switzerland 2 or 3 days prior to the floods contribute to the flood events. It is possible that after a dry period, an AR causing heavy precipitation in Switzerland leads to the filling of the aquifers, but does not produce significant river runoff. However, a few days later a storm occurs, which produces again heavy precipitation. Since the soil is already saturated in water from the AR event, it could result in high river runoff, which could in turn lead to flooding. Watershed properties and preexisting soil moisture could thus play a role on the flood response to precipitation caused by ARs.

Another uncertainty concerns HIAs related to Vb situations. We observed that these moisture fluxes have an influence on floods in Switzerland, especially in spring, summer and fall (Section 4.3.2.2). According to (Schmocker-Fackel and Naef, 2010), Vb situations are mostly responsible for floods in central Switzerland. While some of these structures were detected by the algorithm, we also noted that not all of them were detected due to their

small size (Section 4.3.1). Due to the under-detection of HIAs related to Vb situations, the proportion of these events related to Swiss floods could be higher than what was mentioned in the present study.

Finally, the composite plots presented in Section 4.3.2.4 allowed the identification of different pressure, θ_e and PV conditions that could explain the occurrence of ARs over Switzerland prior to flood events. While each event should be analyzed individually, the composite plots provide a first insight on the synoptic situations responsible for AR activity above the country. In particular, we noted a strong pressure gradient over western Europe in winter, causing the air to flow in a westerly flow towards Switzerland, as well as the presence of a PV trough over western France in summer and fall, forcing the air in a SW flow towards Switzerland.

5.4 Relation between atmospheric rivers and extratropical cyclones

The examination of a case study of the winter season December 1989 - February 1990 allowed us to gain a preliminary insight on the relation between ARs and extratropical cyclones, by investigating the relation between ARs, fronts and WCBs, which is discussed in the following sections.

5.4.1 Atmospheric rivers and fronts

The evaluation of the overlap method showed that the method was able to detect ARs overlapping with frontal structures. However, it showed limitations in the ability to detect fronts overlapping with ARs, suggesting that frontal patterns should be slightly enlarged (e.g. by 1 grid point), in order to increase the probability of overlap. This could also be achieved by using another detection scheme. For example, we saw in Section 4.1 that detection scheme IVT_{250} detects larger structures than IVT_{350}. By using this scheme, the overlap between fronts and ARs would be increased.

The analysis of the case study for the winter 1989-1990 showed that all the ARs observed at that season were related to frontal structures. Most ARs seemed to be associated with

an extratropical cyclone located at the head of the AR, with clearly visible cold and warm fronts. Only three ARs did not show a clear relation with extratropical cyclones, occurring rather in the strong westerly flow south of low pressure systems. While frontal structures were observed on their northwestern flanks, they could not be associated with the frontal patterns of an extratropical cyclone. Therefore, even though this season might not be representative of all winter seasons, these findings suggest that most winter-time ARs are related to extratropical cyclones, as described in the literature (Ralph et al., 2004, 2005; Bao et al., 2006; Ralph and Dettinger, 2011; Gimeno et al., 2014). These findings also agree with observations made earlier (Section 5.2), where we noted that the spatial patterns of the AR climatology are very similar to those of the storm tracks climatology (Hoskins and Hodges, 2002). However, one should note that the front detection method based on the gradient of θ_e at 850 hPa detects regions of strong moisture gradient (Schemm et al., 2014), resulting in the detection of fronts on the sides or at the head of ARs, where the θ_e gradient is important. Using another front detection method, for example one based on the potential temperature θ, could result in the detection of different frontal patterns and the observation of a weaker relation between fronts and ARs.

Furthermore, we observed in some cases that the ARs were related to two cyclonic systems. Similar observations were made by Sodemann and Stohl (2013), who found that ARs observed during one winter month could be related to multiple cyclones, depending on the wave breaking pattern and the orientation of the upper-level jet. Indeed, a meridionally oriented jet is associated with the formation of several small short lived cyclones, while a zonally oriented jet is typically associated with the formation of one large and long lasting cyclone (Sodemann and Stohl, 2013). They suggested that the relation between ARs and multiple cyclones could have an importance on the precipitation amount, since the presence of several cyclones along the AR would allow a much higher moisture transport than by a single cyclone.

Finally, we did not observe any frontal patterns or signs of extratropical cyclones in proximity to HIAs with the front data resulting from the earlier version of the front detection algorithm of Schemm et al. (2014). However, when plotting fronts using the more recently produced data, small fronts were observed on the northwestern flank of the tails of some HIAs. These differences arise from the fact that both versions set different criteria as minimum length, respectively 10 grid points for the earlier version and 500 km for the more recent version. Hence, with these observations, it could be possible that HIAs over the Mediterranean Sea are the equivalent of ARs over the North Atlantic, only at a smaller scale, and are related to smaller frontal patterns. However, further studies would be needed to investigate this hypothesis.

5.4.2 Atmospheric rivers and warm conveyor belts

The analysis of the case study for the winter 1989-1990 showed that no WCBs were observed in proximity to HIAs, which is not surprising since we found that they were often not associated with extratropical cyclones and frontal patterns. In contrast, in most cases WCBs were observed at the head or in the middle of the ARs over the western North Atlantic. The ascending WCBs were related to extratropical cyclones with developed frontal systems. This suggests a strong link between ARs and WCBs in the development phase of extratropical cyclones over the western North Atlantic. Over the eastern North Atlantic, however, a weaker relation was observed. As the WCBs were taken into the cyclonic circulation of the extratropical cyclones, one third of the ARs showed rapid dissipation (e.g. case of 23-25 December 1989). This behavior supports the idea according to which ARs form a subsection of the WCBs of extratropical cyclones in which strong latent heat transport occurs (e.g. Ralph et al., 2004, 2011; Lavers et al., 2012). According to this view, an AR is mainly formed through local moisture convergence within the WCB and along the trailing cold front of the cyclone (Bao et al., 2006; Cordeira et al., 2013; Neiman et al., 2013). The head of the WCB constitutes the leading edge of the AR, since moisture is precipitated with the ascent of the air in the WCB (Stohl et al., 2008). As the WCB is taken into the cyclonic circulation of the extratropical cyclone, we observed that the associated frontal system progressively disappears. The decrease of frontogenesis could explain why the AR gradually dissipates; the absence of sufficient moisture convergence within the frontal zone does not compensate anymore for the loss of moisture through precipitation in the ascending air within the WCB.

However, we also observed that two thirds of the ARs seemed to become decoupled from the WCBs over the eastern North Atlantic. While the WCBs were taken into the cyclonic circulation of the extratropical cyclones, the ARs continued their path eastwards in the westerly flow south of the extratropical cyclones to which they were associated (e.g. case of 18-20 February 1990). These findings contradict with the traditional view of the relation between ARs and WCBs presented above. While ARs and WCBs seem to evolve together and to be closely related, they should be distinguished from one another. This assumption is supported by other authors (e.g. Knippertz and Martin, 2007; Sodemann and Stohl, 2013). To stress the differences between both processes that nevertheless show a similar motion, Knippertz and Martin (2007) suggest to qualify AR structures as "moisture conveyor belts". While the term "atmospheric river" suggests a two dimensional movement, the term "moisture conveyor belt" indicates a three-dimensional ascent, similar to the ascent of WCBs of the well-known conveyor belt model of extratropical cyclones and better represents the transport of moisture occurring within ARs.

While we found that some ARs become decoupled from the related WCBs over the eastern North Atlantic, the mechanisms responsible for the persistence of the ARs after their separation with the WCBs remain unclear. We observed that after the separation, the ARs continue their path eastwards in the westerly flow south the of associated extratropical cyclones. It is possible that less ascent inside the ARs compared to the WCBs leads to less moisture depletion through precipitation, allowing the ARs to persist in time. The presence of an anticyclone over Europe could increase the pressure gradient and thus the westerly circulation, pushing the ARs towards the European continent. Another explanation could be found in the development of secondary extratropical cyclones along the ARs. For the case of 18-20 February 1990, we observed frontal patterns similar to those of an extratropical cyclone developing on the northwestern flank of the AR, as well as a distortion in the wind field, suggesting the presence of a developing cyclone. Moisture convergence within the frontal zone of this secondary cyclone (Bao et al., 2006; Cordeira et al., 2013; Neiman et al., 2013) could feed the leading end of the AR, allowing it to persist in time (Sodemann and Stohl, 2013). However, further studies would be needed in order to investigate this proposition.

Chapter 6

Conclusion

In the past years, several studies have focused on defining the characteristics of atmospheric rivers (ARs) and have used these definitions to detect ARs in different datasets. While most studies have focused on North Pacific ARs, this master's thesis focused on ARs occurring over the North Atlantic Ocean and Europe. In a first stage, an algorithm was developed to detect ARs in the ERA-Interim dataset for the period 1979-2011. It consisted of four detection schemes, which detected ARs according to various criteria (total precipitable water, wind speed, integrated vapor transport and area). Some schemes showed good detection of ARs over the ocean (fixed-threshold-based schemes), while others showed good detection over the land (percentile-based schemes). In addition, not only did the algorithm detect ARs, but it also detected smaller structures that we named HIAs (high IVT areas). HIAs have similar characteristics than ARs but have a shorter length (< 2000 km). However, since they can bring considerable amounts of moisture towards the land and can participate to the triggering of heavy precipitation events, they are also of interest when studying moisture fluxes towards the continent.

Using the algorithm output, the seasonal climatological frequency of ARs and HIAs was computed for the period 1979-2011, where special attention was given to the North Atlantic Ocean and European continent. The climatology showed a strong resemblance with the storm track climatology over the North Atlantic. In addition, percentile-based schemes showed higher AR/HIA frequency in winter and fall, while fixed-threshold-based schemes showed higher activity in summer and fall. These differences highlight the sensitivity of the fixed-threshold-based schemes to seasonal changes in the moisture content of the air. Furthermore, the AR frequency maxima showed a seasonal shift, with a zonal orientation in

summer and fall and a SW-NE tilted orientation in winter and spring, suggesting different moisture sources depending on the season. ARs in winter and spring seem to originate in the tropics, while summer and fall-time ARs seem to originate in extratropical regions.

Next, the seasonal and regional influence of ARs on flood events in Switzerland was investigated through the study of the fourteen largest floods that occurred in the country between 1979 and 2011, as well as with the analysis of smaller flood events. We found that the regional and seasonal influence of ARs/HIAs on the occurrence of floods in Switzerland could be explained to a certain extent by the topography and the direction of the flow. Two regions are sensitive to ARs/HIAs depending on the season. The Jura (NW Switzerland) is affected by ARs/HIAs arriving in westerly flows in winter and spring, while ARs/HIAs from the SW affect mostly Ticino (S Switzerland) in fall and summer. HIAs related to Vb situations, which play an important role for floods in central Switzerland, could not be analyzed precisely, since the algorithm detects only some but not all of these structures due to their too small size.

Finally, the relation between ARs and extratropical cyclones was investigated through the analysis of the winter December 1989 to February 1990. Findings showed that most ARs were associated with extratropical cyclones that had developed frontal systems and warm conveyor belts (WCBs). While ARs and WCBs were closely linked over the western North Atlantic, they showed a weaker relation over the eastern North Atlantic. Indeed, two thirds of the ARs observed during that season seemed to become decoupled from the WCBs and continued their path eastwards in the westerly flow south of the extratropical cyclones to which they were associated. These findings contradict the traditional view according to which ARs form a subsection of the WCBs of extratropical cyclones and suggest that while ARs and WCBs seem to evolve together and are closely related, they are distinct features that should be distinguished from one another. In addition, we also found that many ARs are not related to only one extratropical cyclone, but can sometimes be associated with multiple cyclones. Extratropical cyclones are of particular importance for ARs by providing moisture through moisture convergence in the WCB and along the cold front. Multiple cyclones could allow the ARs to persist in time and to transport considerable amounts of moisture towards the mid-latitudes.

Chapter 7

Outlook

In this final section, ideas for further research are presented.

- First of all, further investigation could be conducted on HIAs (high IVT areas), in particular to see if they are the equivalent of ARs at a smaller scale over the Mediterranean or if they are related to other processes. HIAs are of particular interest since they were found to be related to some flood events in Switzerland. To assess the relative proportion of HIAs and ARs in the AR/HIA climatology, the algorithm could be modified by adding a length criterion, discriminating features smaller than 2000 km. A climatology of ARs could then be computed and compared with the AR/HIA climatology presented in Section 4.2. Differences would show the relative influence of HIAs. In addition, case studies as in Section 4.4 could be conducted, in particular for the spring, summer and fall seasons, when HIAs are more frequent.

- HIAs related to Vb situations could also be further analyzed, to assess their influence on flood events in Switzerland. For example, plots of moisture fluxes could be created for days prior to the flood events for which no AR/HIA characteristics were observed. It is possible that some of these events were caused by HIAs related to Vb situations, since the algorithm does not always detect these patterns due to their small size.

- The influence of ARs over Switzerland a few days before the flood events remains unclear and could be the focus of further research. For example, frequency plots for 2 to 3 days prior to the floods could be created, similar to the one presented in Section 4.3.2.2, in order to evaluate the influence of the ARs on the flood events. In addition, since our findings concerning the influence of ARs on Swiss floods are based on a previous regional classification of the measure stations, it should be verified that similar results would be obtained with the more recent classification of Froidevaux (2014).

- Furthermore, the synoptic situations responsible for the occurrence of ARs and HIAs over Switzerland on flood days could be investigated by analyzing individual events. Knowing the atmospheric precursors for floods in Switzerland would be of high interest for the prediction of floods. If the analysis of weather maps can predict that an AR/HIA will cross the country and could produce heavy precipitation, measures could be taken in order to reduce the impacts of such an event in the concerned regions and avoid potentially damaging floods. However, this also requires the knowledge of the responses of the different watershed basins to precipitation.

- The algorithm could also be applied to a longer dataset, to investigate if the frequency of occurrence of ARs or the proportion of flood-related ARs have changed over time. In addition, the algorithm output could be used to link past extreme precipitation or flood events observed in climate proxies such as ice cores or tree rings to the presence of ARs over a given region at a given time and provide understanding for such events.

- Understanding the relation between ARs and WCBs and why some ARs seem to become decoupled from the associated WCBs over the eastern North Atlantic could also be a starting point for further research. The role of anticyclones over Europe, creating a strong pressure gradient and a strong westerly flow, or the role of multiple cyclones along the ARs could be investigated.

- The AR/HIA climatology showed a seasonal shift in AR/HIA patterns over the North Atlantic, suggesting different moisture sources depending on the season. The investigation of moisture sources could also be the focus of future studies, which could be done by performing trajectory analysis (e.g. Bao et al., 2006; Stohl et al., 2008; Sodemann et al., 2008; Knippertz and Wernli, 2010) or water budget studies (e.g. Cordeira et al., 2013). This would allow to understand where the moisture composing ARs comes from and the relative contribution of direct poleward moisture transport from the tropics and that of moisture convergence through frontogenesis. While these have been studied for North Pacific ARs, only few case studies have been conducted over the North Atlantic for specific regions.

- Finally, one can mention the work of Neiman et al. (2008b), who developed a catalogue of all landfalling ARs on the west coast of North America for 1997-2005. While several studies on ARs have been conducted in Europe (e.g. Stohl et al., 2008; Lavers et al., 2011, 2012; Sodemann and Stohl, 2013), they have only focused on ARs occurring in given regions. Lavers and Villarini (2013) studied the relation between ARs and extreme precipitation in Europe, however no catalogue similar to the one of Neiman et al. (2008b) has been produced. Such a catalogue could serve as a basis for further analysis, for e.g. to study the influence of ARs on flood events in different European countries.

Bibliography

Bao, J. W., Michelson, S. A., Neiman, P. J., Ralph, F. M., and Wilczak, J. M. (2006). Interpretation of enhanced integrated water vapor bands associated with extratropical cyclones: Their formation and connection to tropical moisture. *Monthly Weather Review*, *134*(4), 1063–1080.

Berrisford, P., Dee, D. P., Fielding, K., Fuentes, M., Kallberg, P., Kobayashi, S., Uppala, S., et al. (2009). The ERA-Interim archive. *ERA report series*, (1), 1–16.

Browning, K. and Pardoe, C. (1973). Structure of low-level jet streams ahead of mid-latitude cold fronts. *Quarterly Journal of the Royal Meteorological Society*, *99*(422), 619–638.

Byna, S., Prabhat, Wehner, M. F., and Wu, K. J. (2011). Detecting atmospheric rivers in large climate datasets. In *Proceedings of the 2nd international workshop on Petascal data analytics: challenges and opportunities*, pages 7–14.

Cooperative Institute for Meterological Satellite Studies, Tropical Cyclones Group (2014). *Morphed Integrated Microwave Imagery at CIMSS - Total Precipitable Water (MIMIC-TPW) [Online].* Available at http://tropic.ssec.wisc.edu/real-time/mimic-tpw/global/main.html (accessed 15 July 2014).

Cordeira (2014). *Atmospheric rivers [Online].* Available at http://jasoncordeira.weebly.com/atmospheric-rivers.html (accessed 17 July 2014).

Cordeira, J. M., Ralph, F. M., and Moore, B. J. (2013). The development and evolution of two atmospheric rivers in proximity to western North Pacific tropical cyclones in October 2010. *Monthly Weather Review*, *141*(12), 4234–4255.

Dee, D. P., Uppala, S. M., Simmons, A. J., Berrisford, P., Poli, P., Kobayashi, S., Andrae, U., et al. (2011). The ERA-Interim reanalysis: Configuration and performance of the data assimilation system. *Quarterly Journal of the Royal Meteorological Society*, *137*(656), 553–597.

Dettinger, M. D. (2011). Climate change, atmospheric rivers, and floods in California – A multimodel analysis of storm frequency and magnitude changes. *Journal of the American Water Resources Association*, *47*(3), 514–523.

Fink, A. H. and Knippertz, P. (2003). An extreme precipitation event in southern Morocco in spring 2002 and some hydrological implications. *Weather*, *58*(10), 377–387.

Froidevaux, P. (2014). *Meteorological characterisation of floods in Switzerland*. PhD thesis, University of Bern, Faculty of Science. In preparation.

Gimeno, L., Nieto, R., Vázquez, M., and Lavers, D. A. (2014). Atmospheric rivers: a mini-review. *Frontiers in Earth Science*, *2*, 1–6.

Godard, A. and Tabeaud, M. (2009). *Les climats: Mécanismes, variabilités, répartition (4^{th} Rev. Ed.)*. Paris: A. Colin.

Hoskins, B. J. and Hodges, K. I. (2002). New perspectives on the Northern Hemisphere winter storm tracks. *Journal of the Atmospheric Sciences*, *59*(6), 1041–1061.

Jankov, I., Bao, J. W., Neiman, P. J., Schultz, P. J., Yuan, H., and White, A. B. (2009). Evaluation and comparison of microphysical algorithms in ARW-WRF model simulations of atmospheric river events affecting the California coast. *Journal of Hydrometeorology*, *10*(4), 847–870.

Knippertz, P. and Martin, J. E. (2005). Tropical plumes and extreme precipitation in subtropical and tropical West Africa. *Quarterly Journal of the Royal Meteorological Society*, *131*(610), 2337–2365.

Knippertz, P. and Martin, J. E. (2007). A Pacific moisture conveyor belt and its relationship to a significant precipitation event in the semiarid southwestern United States. *Weather and Forecasting*, *22*(1), 125–144.

Knippertz, P. and Wernli, H. (2010). A Lagrangian climatology of tropical moisture exports to the Northern Hemispheric extratropics. *Journal of Climate*, *23*(4), 987–1003.

Knippertz, P., Wernli, H., and Gläser, G. (2013). A global climatology of tropical moisture exports. *Journal of Climate*, *26*(10), 3031–3045.

Lavers, D. and Villarini, G. (2013). The nexus between atmospheric rivers and extreme precipitation across Europe. *Geophysical Research Letters*, *40*(12), 3259–3264.

Lavers, D. A., Allan, R. P., Villarini, G., Lloyd-Hughes, B., Brayshaw, D. J., and Wade, A. J. (2013). Future changes in atmospheric rivers and their implications for winter flooding in Britain. *Environmental Research Letters*, *8*(3), 034010.

Lavers, D. A., Allan, R. P., Wood, E. F., Villarini, G., Brayshaw, D. J., and Wade, A. J. (2011). Winter floods in Britain are connected to atmospheric rivers. *Geophysical Research Letters*, *38*(23), L23803.

Lavers, D. A., Villarini, G., Allan, R. P., Wood, E. F., and Wade, A. J. (2012). The detection of atmospheric rivers in atmospheric reanalyses and their links to British winter floods and the large-scale climatic circulation. *Journal of Geophysical Research: Atmospheres (1984-2012)*, *117*(D20).

Leung, L. R. and Qian, Y. (2009). Atmospheric rivers induced heavy precipitation and flooding in the western U.S. simulated by the WRF regional climate model. *Geophysical Research Letters*, *36*(3).

Madonna, E., Wernli, H., Joos, H., and Martius, O. (2014). Warm conveyor belts in the ERA-Interim dataset (1979–2010). Part I: Climatology and potential vorticity evolution. *Journal of Climate*, *27*(1), 3–26.

Massacand, A. C., Wernli, H., and Davies, H. C. (1998). Heavy precipitation on the alpine southside: An upper-level precursor. *Geophysical Research Letters*, *25*(9), 1435–1438.

Moore, B. J., Neiman, P. J., Ralph, F. M., and Barthold, F. E. (2012). Physical processes associated with heavy flooding rainfall in Nashville, Tennessee, and vicinity during 1–2 May 2010: The role of an atmospheric river and mesoscale convective systems. *Monthly Weather Review*, *140*(2), 358–378.

Neiman, P. J., Ralph, F. M., Moore, B. J., Hughes, M., Mahoney, K. M., Cordeira, J. M., and Dettinger, M. D. (2013). The landfall and inland penetration of a flood-producing atmospheric river in Arizona. Part I: Observed synoptic-scale, orographic, and hydrometeorological characteristics. *Journal of Hydrometeorology*, *14*(2), 460–484.

Neiman, P. J., Ralph, F. M., Wick, G. A., Kuo, Y.-H., Wee, T.-K., Ma, Z., Taylor, G. H., and Dettinger, M. D. (2008a). Diagnosis of an intense atmospheric river impacting the Pacific Northwest: Storm summary and offshore vertical structure observed with COSMIC satellite retrievals. *Monthly Weather Review*, *136*(11), 4398–4420.

Neiman, P. J., Ralph, F. M., Wick, G. A., Lundquist, J. D., and Dettinger, M. D. (2008b). Meteorological characteristics and overland precipitation impacts of atmospheric rivers affecting the west coast of North America based on eight years of SSM/I satellite observations. *Journal of Hydrometeorology*, *9*(1), 22–47.

Neiman, P. J., Schick, L. J., Ralph, F. M., Hughes, M., and Wick, G. A. (2011). Flooding in Western Washington: The connection to atmospheric rivers. *Journal of Hydrometeorology*, *12*(6), 1337–1358.

Newell, R. E., Newell, N. E., Zhu, Y., and Scott, C. (1992). Tropospheric rivers? - A pilot study. *Geophysical Research Letters*, *19*(24), 2401–2404.

Ralph, F. M. and Dettinger, M. D. (2011). Storms, floods, and the science of atmospheric rivers. *Eos, Transactions American Geophysical Union*, *92*(32), 265–266.

Ralph, F. M. and Dettinger, M. D. (2012). Historical and national perspectives on extreme West Coast precipitation associated with atmospheric rivers during December 2010. *Bulletin of the American Meteorological Society*, *93*(6), 783–790.

Ralph, F. M., Neiman, P. J., Kiladis, G. N., Weickmann, K., and Reynolds, D. W. (2011). A multiscale observational case study of a Pacific atmospheric river exhibiting tropical–extratropical connections and a mesoscale frontal wave. *Monthly Weather Review*, *139*(4), 1169–1189.

Ralph, F. M., Neiman, P. J., and Rotunno, R. (2005). Dropsonde observations in low-level jets over the northeastern Pacific Ocean from CALJET-1998 and PACJET-2001: Mean vertical-profile and atmospheric-river characteristics. *Monthly Weather Review*, *133*(4), 889–910.

Ralph, F. M., Neiman, P. J., and Wick, G. A. (2004). Satellite and CALJET aircraft observations of atmospheric rivers over the eastern North Pacific Ocean during the winter of 1997/98. *Monthly Weather Review*, *132*(7), 1721–1745.

Ralph, F. M., Neiman, P. J., Wick, G. A., Gutman, S. I., Dettinger, M. D., Cayan, D. R., and White, A. B. (2006). Flooding on California's Russian River: Role of atmospheric rivers. *Geophysical Research Letters*, *33*(13).

Rutz, J. J., Steenburgh, W. J., and Ralph, F. M. (2014). Climatological characteristics of atmospheric rivers and their inland penetration over the western United States. *Monthly Weather Review*, *142*(2), 905–921.

Schemm, S., Rudeva, I., and Simmonds, I. (2014). Extratropical fronts in the lower troposphere - Global perspectives obtained from two automated methods. *Quarterly Journal of the Royal Meteorological Society*. In review.

Schmocker-Fackel, P. and Naef, F. (2010). More frequent flooding? Changes in flood frequency in Switzerland since 1850. *Journal of Hydrology*, *381*(1), 1–8.

Sodemann, H., Schwierz, C., and Wernli, H. (2008). Interannual variability of Greenland winter precipitation sources: Lagrangian moisture diagnostic and North Atlantic Oscillation influence. *Journal of Geophysical Research: Atmospheres (1984-2012)*, *113*(D3).

Sodemann, H. and Stohl, A. (2013). Moisture origin and meridional transport in atmospheric rivers and their association with multiple cyclones. *Monthly Weather Review*, *141*(8), 2850–2868.

Stohl, A., Forster, C., and Sodemann, H. (2008). Remote sources of water vapor forming precipitation on the Norwegian west coast at 60 N – A tale of hurricanes and an atmospheric river. *Journal of Geophysical Research: Atmospheres (1984-2012)*, *113*(D5).

Uppala, S. M., Kållberg, P. W., Simmons, A. J., Andrae, U., Bechtold, V., Fiorino, M., Gibson, J. K., et al. (2005). The ERA-40 re-analysis. *Quarterly Journal of the Royal Meteorological Society*, *131*(612), 2961–3012.

Viale, M. and Nuñez, M. N. (2011). Climatology of winter orographic precipitation over the subtropical central Andes and associated synoptic and regional characteristics. *Journal of Hydrometeorology*, *12*(4), 481–507.

Wallace, J. M. and Hobbs, P. V. (2006). *Atmospheric Science: A Introductory Survey (2nd Ed.)*. Amsterdam: Academic Press.

Zhu, Y. and Newell, R. E. (1998). A proposed algorithm for moisture fluxes from atmospheric rivers. *Monthly Weather Review*, *126*(3), 725–735.

Appendix

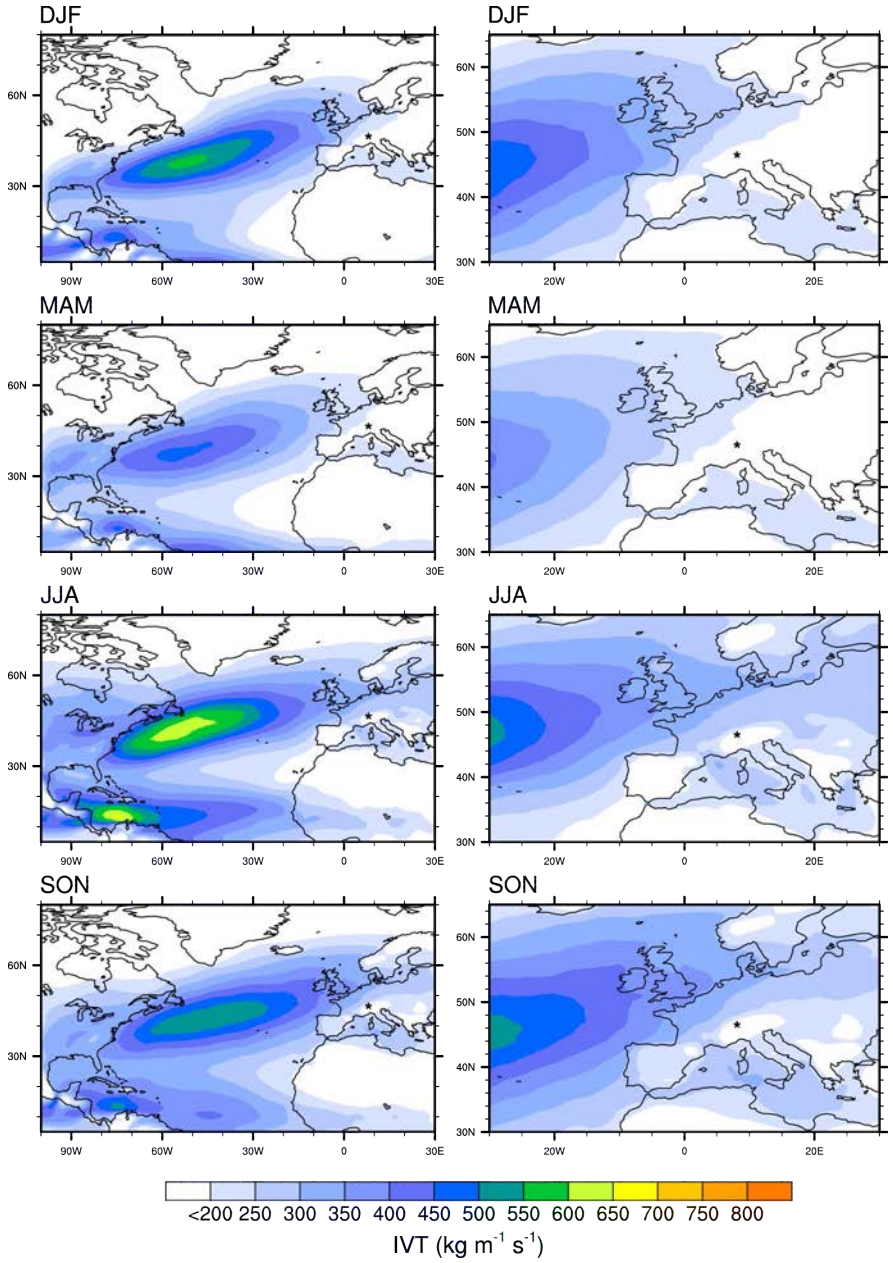

Figure A.1: *85^{th} percentile of seasonal IVT over (a) the North Atlantic and (b) Europe. The star indicates the location of Switzerland.*

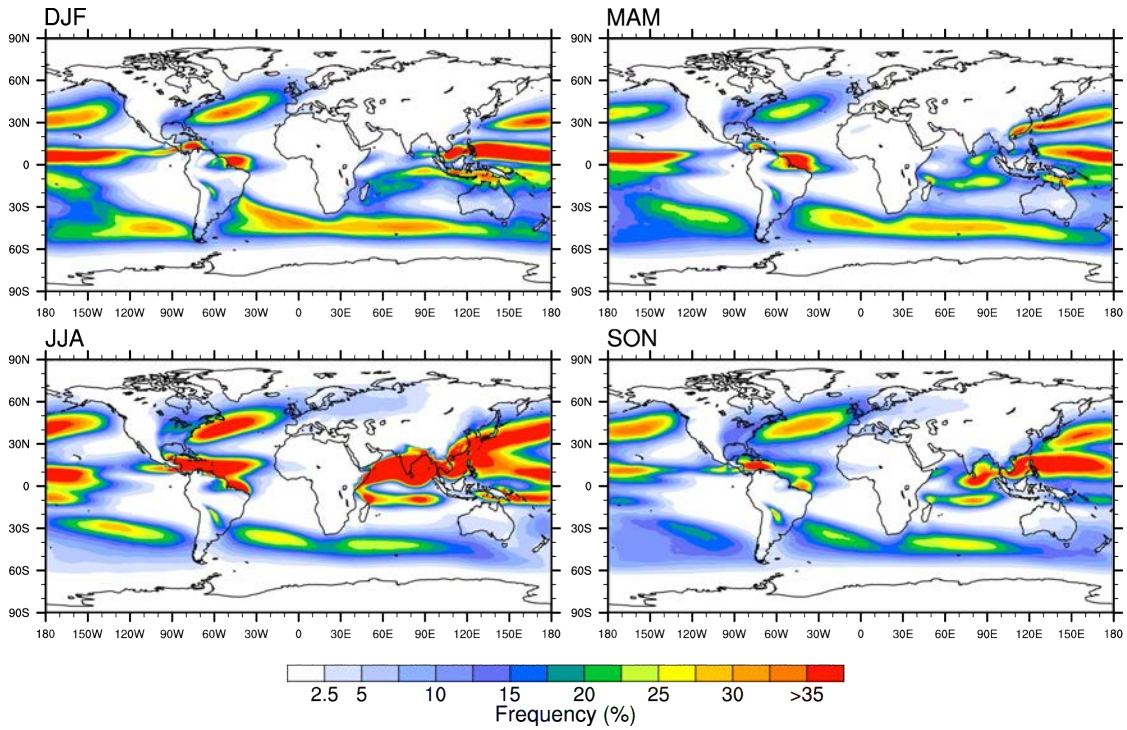

Figure A.2: *Global seasonal frequency of ARs and HIAs for the period 1979-2011 obtained with detection scheme* IVT_{350}.

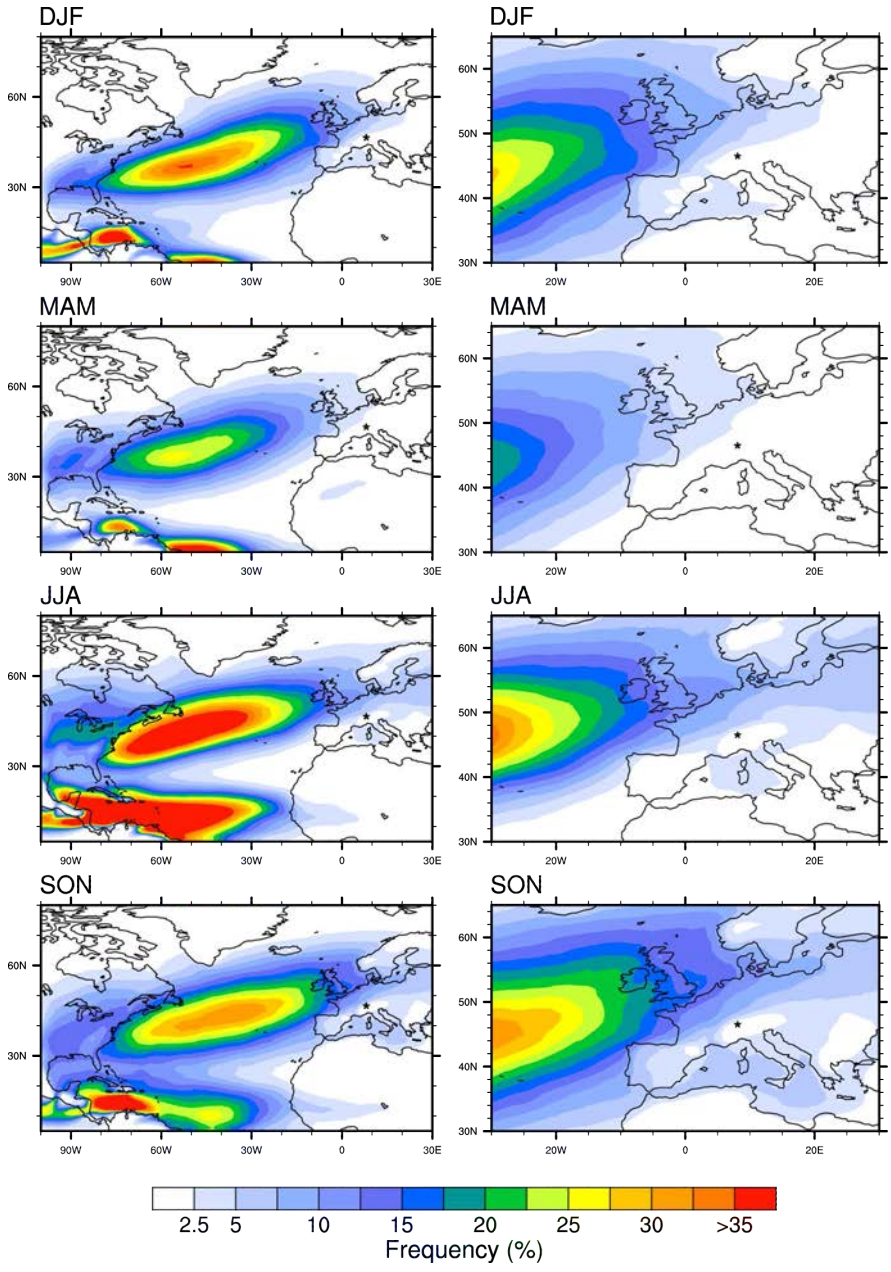

Figure A.3: *Seasonal frequency of ARs and HIAs for the period 1979-2011 for the North Atlantic (left) and Europe (right) obtained with detection scheme* IVT_{350}*. The star indicates the location of Switzerland.*

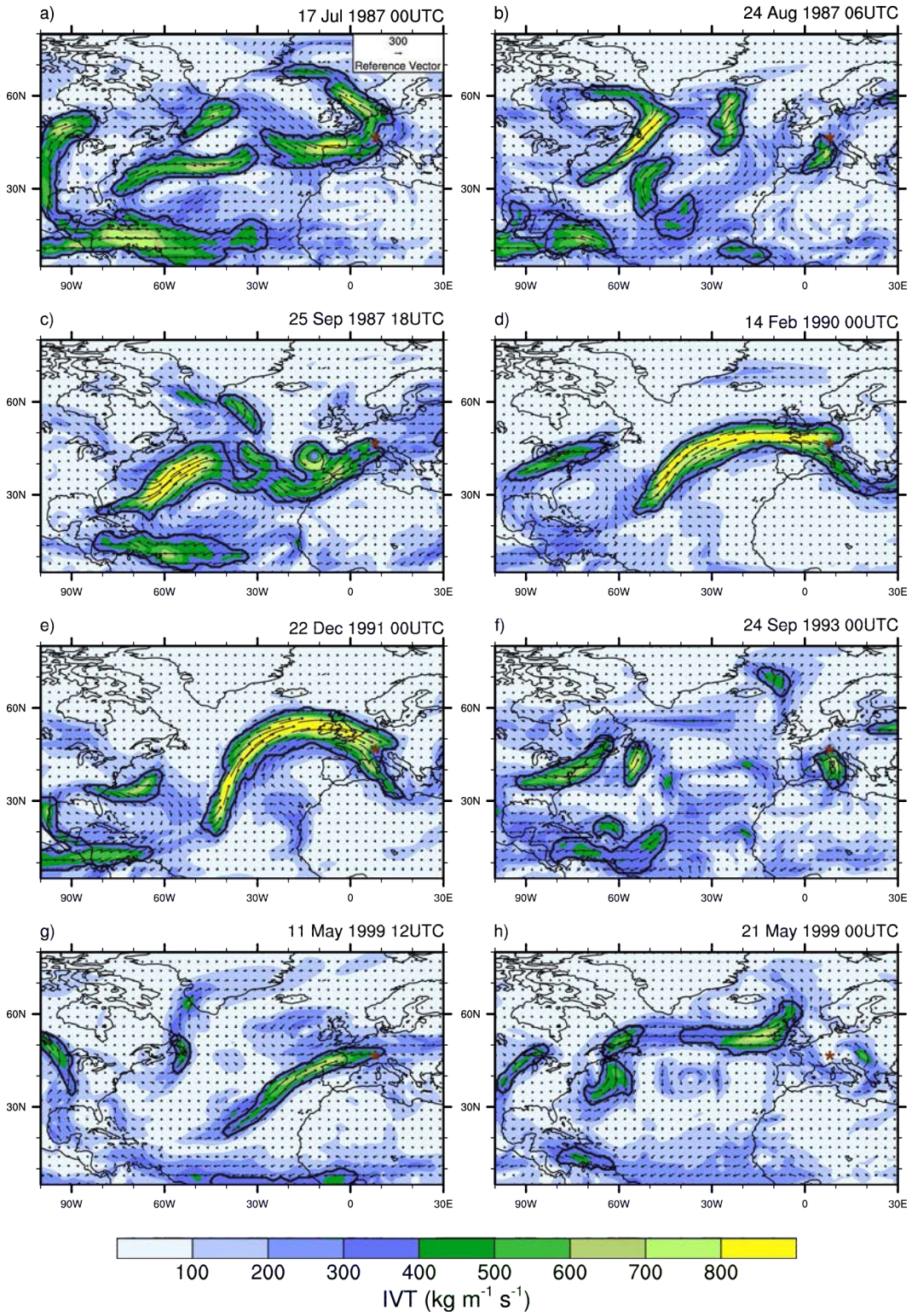

Figure A.4a: *Moisture transport (IVT) over the North Atlantic and Europe prior to the fourteen largest flood events in Switzerland between 1979 and 2011. ARs or high IVT areas detected by detection scheme IVT_{350} are represented in black contour and the overlaid arrows indicate the direction of the IVT. The brown star indicates the location of Switzerland.*

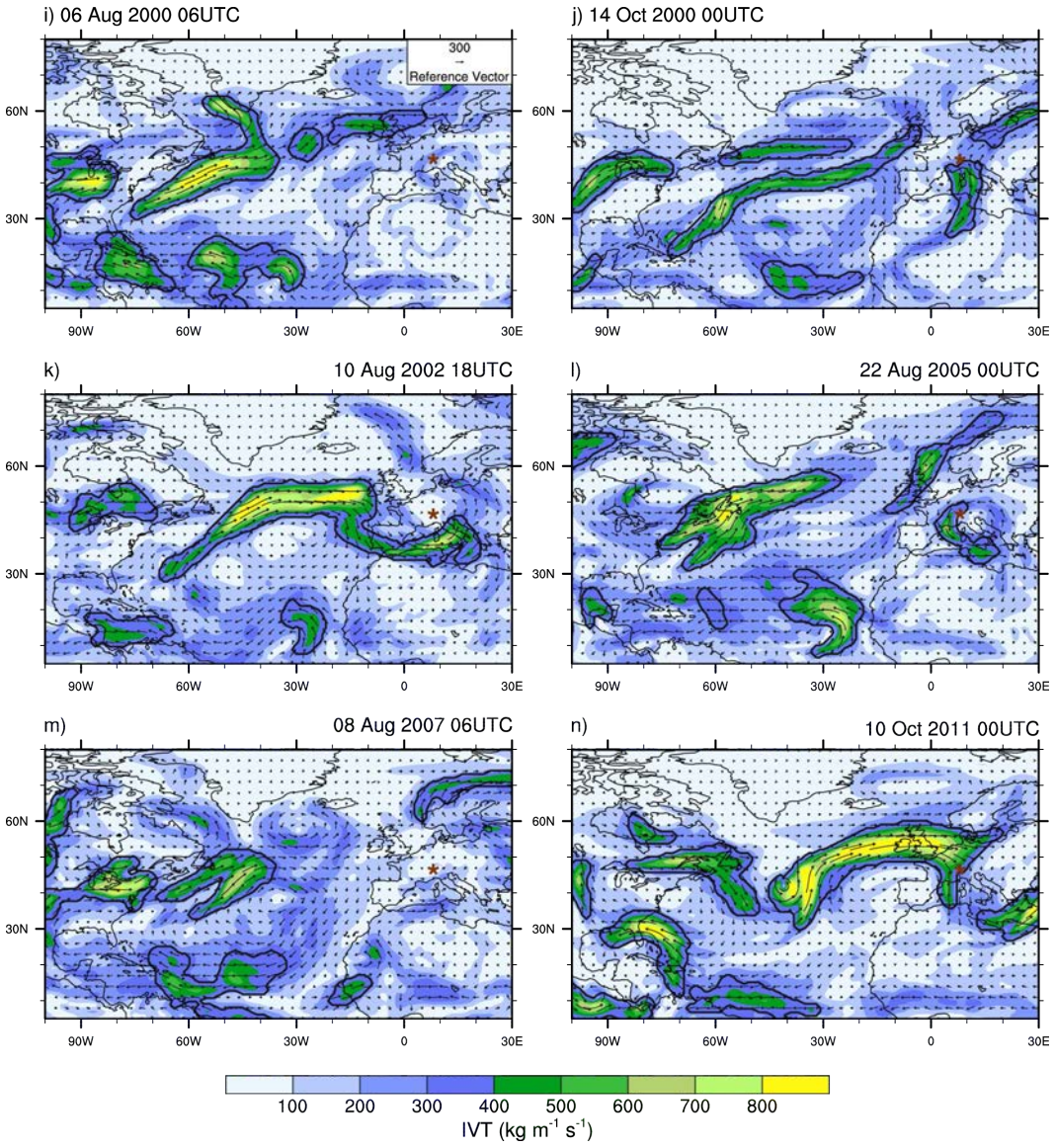

Figure A.4b: *Moisture transport (IVT) over the North Atlantic and Europe prior to the fourteen largest flood events in Switzerland between 1979 and 2011. ARs or high IVT areas detected by detection scheme IVT_{350} are represented in black contour and the overlaid arrows indicate the direction of the IVT. The brown star indicates the location of Switzerland.*

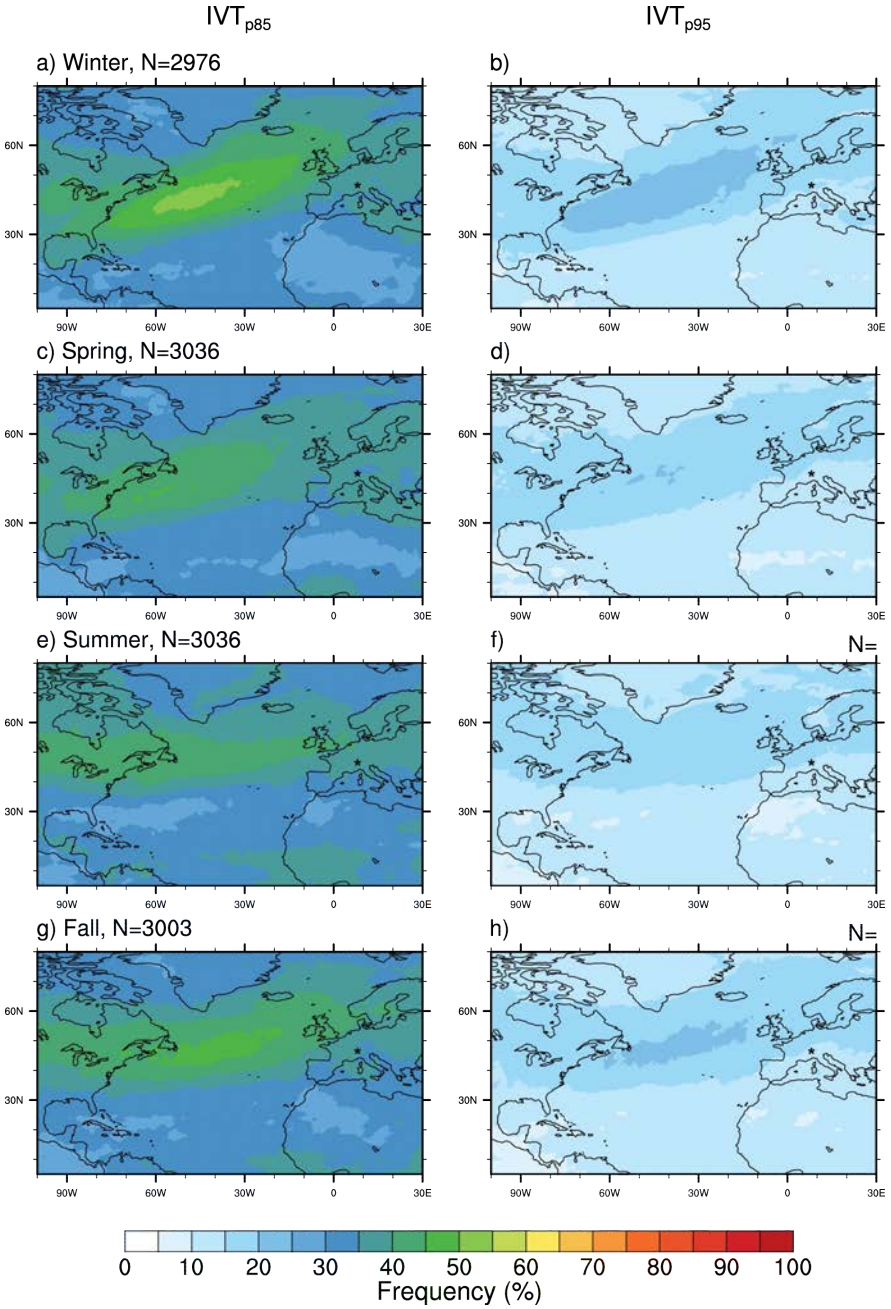

Figure A.5: *Seasonal frequency of ARs and HIAs for the time period 1979-2011 obtained with detection schemes IVT_{p85} (left) and IVT_{p95} (right). The star indicates the location of Switzerland and N the number of events per season.*

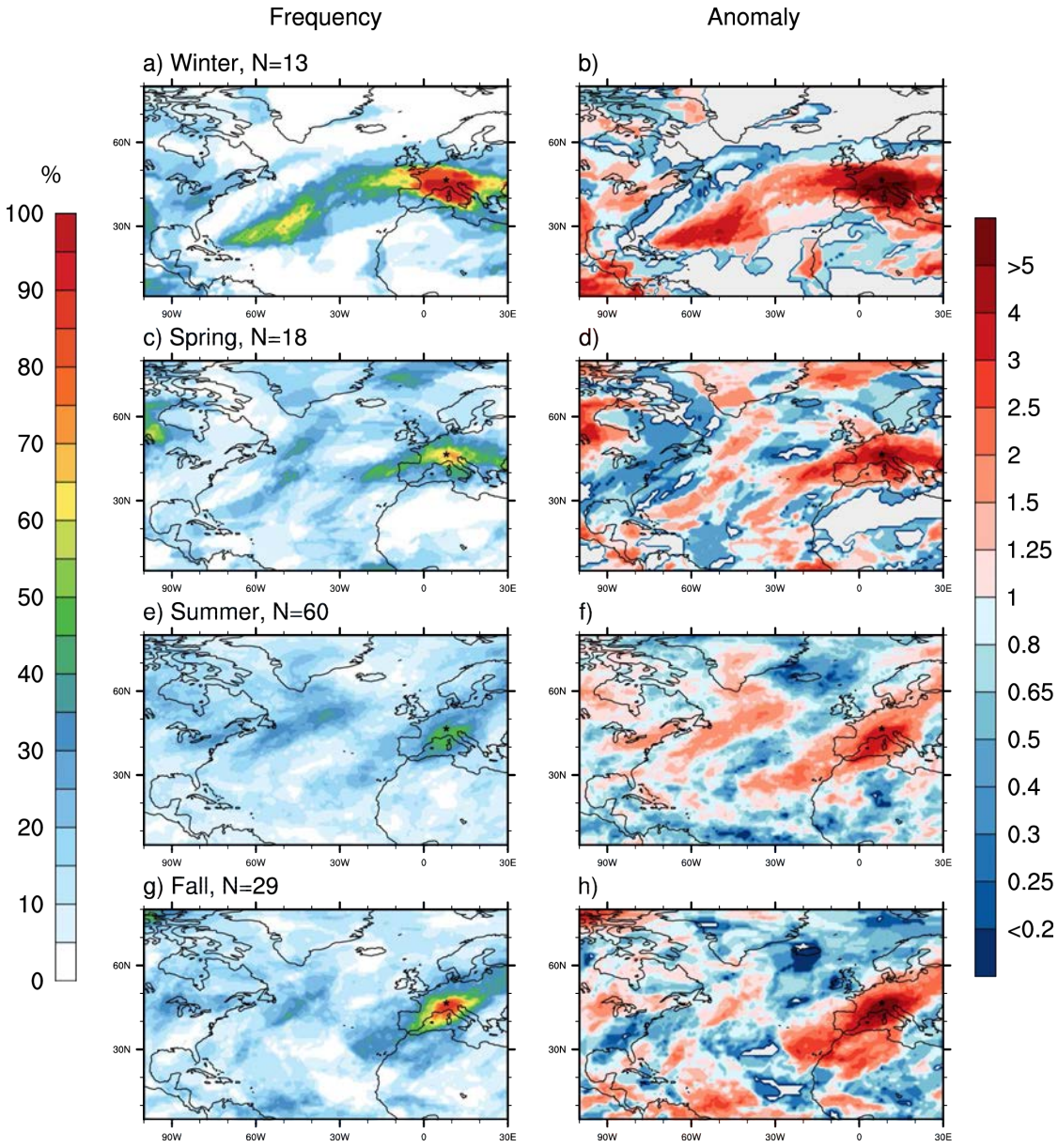

Figure A.6: *Seasonal frequency of ARs and HIAs on the day preceding and the day a flood was recorded in Switzerland obtained with detection scheme IVT_{p95} (left) and anomaly compared to the reference period 1979-2011 (right). Seasonal anomalies were obtained by dividing the frequencies in the left column with the frequencies of the reference period (Appendix Fig. A.5 right). A value of 1 indicates no difference between both frequencies. A value of 2 indicates two times more ARs compared to the reference period. The star indicates the location of Switzerland and N the number of flood days.*

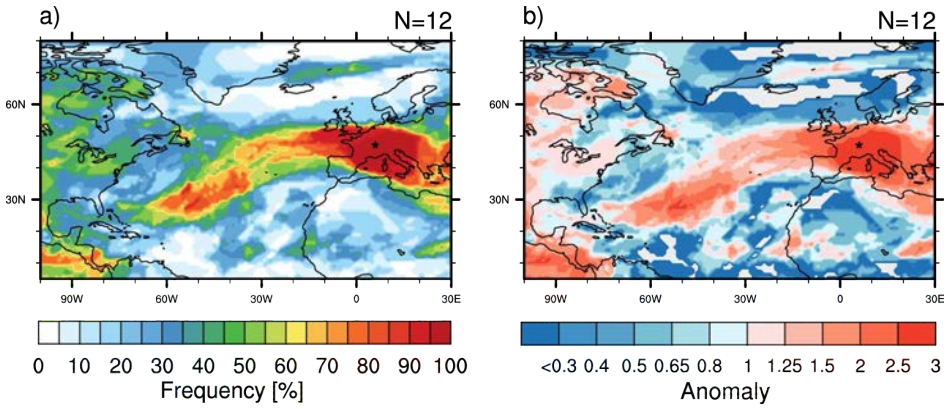

Figure A.7: *Winter-time frequency of ARs and HIAs on the day preceding and the day a flood was recorded in the Jura region obtained with detection scheme IVT_{p85} (left) and anomaly compared to the reference period 1979-2011 (right). The seasonal anomaly was obtained by dividing the frequency in the left column with the frequency of the reference period for the winter season (Appendix Fig. A.5 left). A value of 1 indicates no difference between both frequencies. A value of 2 indicates two times more ARs compared to the reference period. The star indicates the location of the region and N the number of flood days.*

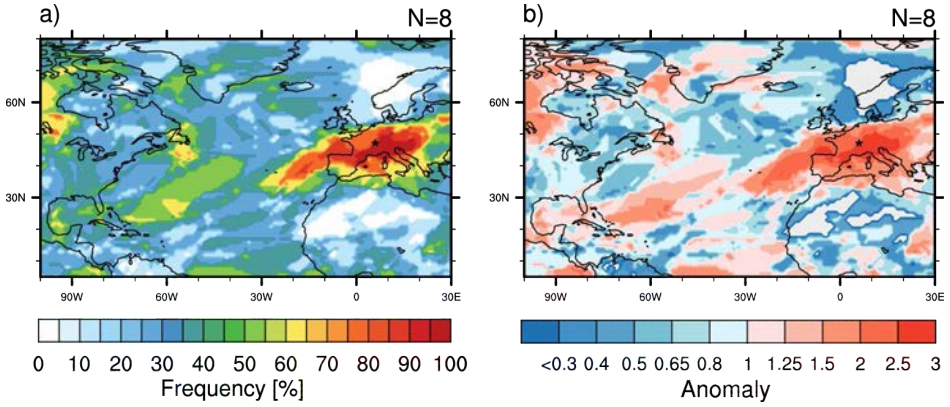

Figure A.8: *Same as Fig. A.7 but for spring-time frequency of ARs and HIAs on the day preceding and the day a flood was recorded in the Jura region.*

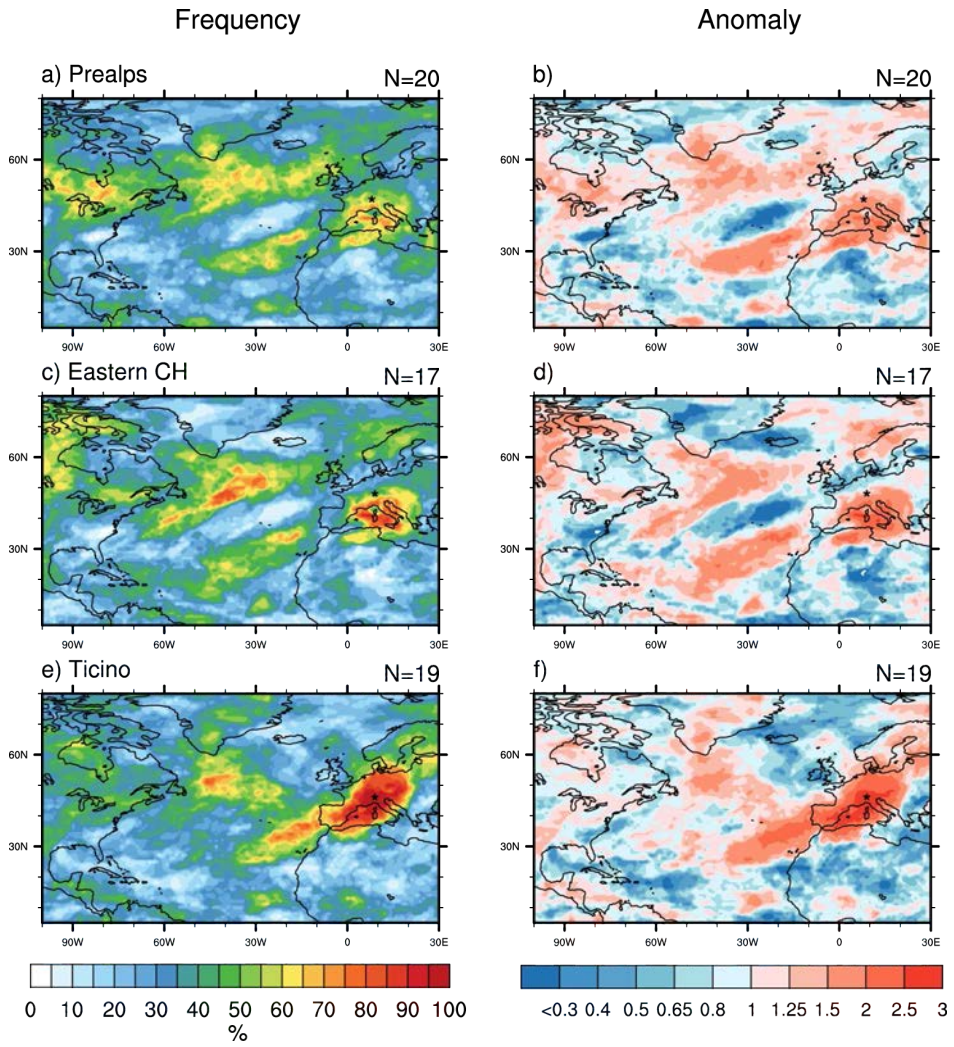

Figure A.9: *Same as Fig. A.7 but for summer-time frequency of ARs and HIAs on the day preceding and the day a flood was recorded in the Prealps, Eastern Switzerland and Ticino regions.*

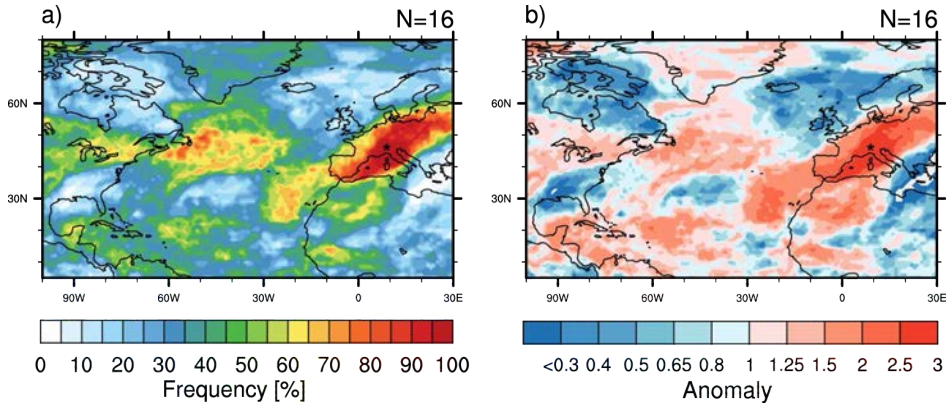

Figure A.10: *Same as Fig. A.7 but for fall-time frequency of ARs and HIAs on the day preceding and the day a flood was recorded in the Ticino region.*

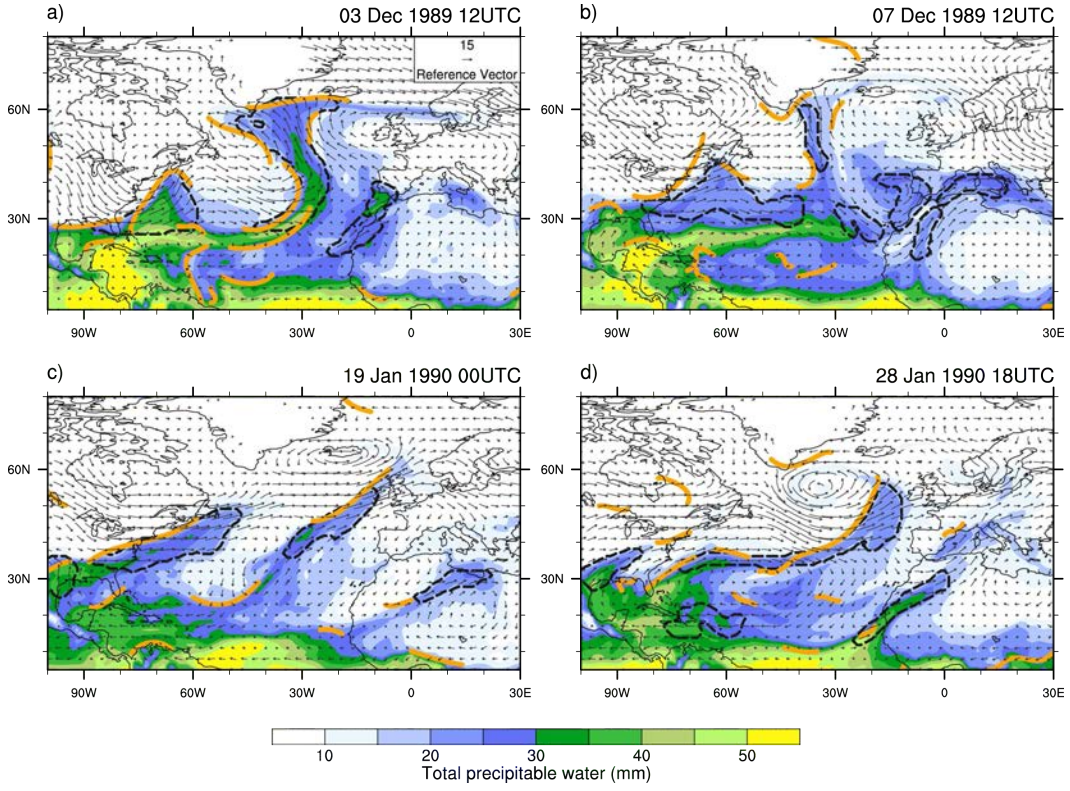

Figure A.11: *HIA cases for the winter season December 1989 to February 1990, with TPW (in color), wind speed at 750 hPa (arrows), ARs detected with the TPW_{20} scheme (dashed black contour) and frontal lines (in orange). Frontal lines are based on a spline interpolation of the front data, courtesy of S. Schemm.*

Declaration

under Art. 28 Para. 2 RSL 05

Last, first name: Fazan, Valérie

Matriculation number: 09-418-237

Programme: M.Sc. in Climate Sciences

Bachelor ☐ Master ☒ Dissertation ☐

Thesis title: North Atlantic atmospheric rivers in the ERA-Interim dataset: Detection, climatology and link to Swiss floods

Thesis supervisor: Prof. Dr. Olivia Romppainen-Martius

I hereby declare that this submission is my own work and that, to the best of my knowledge and belief, it contains no material previously published or written by another person, except where due acknowledgement has been made in the text. In accordance with academic rules and ethical conduct, I have fully cited and referenced all material and results that are not original to this work. I am well aware of the fact that, on the basis of Article 36 Paragraph 1 Letter o of the University Law of 5 September 1996, the Senate is entitled to deny the title awarded on the basis of this work if proven otherwise. I grant inspection of my thesis.

Bern, September 24, 2014

Signature V. Fazan